Leading twist nuclear shadowing, nuclear generalized parton distributions, and nuclear deeply virtual Compton scattering at small x

K. Goeke,[1,*] V. Guzey,[2,†] and M. Siddikov[1,3,4,‡]

[1]*Institut für Theoretische Physik II, Ruhr-Universität-Bochum, D-44780 Bochum, Germany*

[2]*Theory Center, Jefferson Laboratory, Newport News, Virginia 23606, USA*

[3]*Departamento de Física y Centro de Estudios Subatómicos, Universidad Técnica Federico Santa María, Valparaíso, Chile*

[4]*Theoretical Physics Department, Uzbekistan National University, Tashkent 700174, Uzbekistan*

(Received 3 February 2009; published 30 March 2009)

We generalize the leading twist theory of nuclear shadowing and calculate quark and gluon generalized parton distributions (GPDs) of spinless nuclei. We predict very large nuclear shadowing for nuclear GPDs. In the limit of the purely transverse momentum transfer, our nuclear GPDs become impact-parameter-dependent nuclear parton distribution functions (PDFs). Nuclear shadowing induces nontrivial correlations between the impact parameter b and the light-cone fraction x. We make predictions for the deeply virtual Compton scattering (DVCS) amplitude and the DVCS cross section on ^{208}Pb at high energies. We calculate the cross section of the Bethe-Heitler (BH) process and address the issue of the extraction of the DVCS signal from the $eA \to e\gamma A$ cross section. We find that the $eA \to e\gamma A$ differential cross section is dominated by DVCS at the momentum transfer t near the minima of the nuclear form factor. We also find that nuclear shadowing leads to dramatic oscillations of the DVCS beam-spin asymmetry, A_{LU}, as a function of t. The position of the points where A_{LU} changes sign is directly related to the magnitude of nuclear shadowing.

DOI: 10.1103/PhysRevC.79.035210 PACS number(s): 13.60.−r, 24.85.+p

I. INTRODUCTION

Hard exclusive reactions and generalized parton distributions (GPDs) have been at the focus of hadronic physics for the past decade [1–6]. GPDs interpolate between elastic form factors and structure functions and contain detailed information on distributions and correlations of partons (quarks and gluons) in hadronic targets (pions, nucleons, and nuclei). In particular, GPDs describe the distribution of partons both in the longitudinal momentum direction and in the impact parameter (transverse) plane [7] and also allow us to access the total angular momentum of the target carried by the partons [8].

The QCD factorization theorems for hard exclusive processes [9,10] state that GPDs are universal distributions that enter the perturbative QCD description of various hard exclusive processes such as deeply virtual Compton scattering (DVCS), $\gamma^* T \to \gamma T$ (where T denotes any hadronic target), exclusive production of mesons, $\gamma^* T \to M T$ [where M denotes a (pesudo)scalar or a vector meson], and many other processes, including generalizations of these two reactions.

Although the factorization theorems make it theoretically possible to extract GPDs from the data, this is a difficult task in practice since GPDs are functions of four variables and the GPDs enter experimentally measured observables in the form of convolution with hard coefficient functions. Therefore, there is a clear need for modeling GPDs, both to interpret the results of the completed experiments in terms of the microscopic structure of the hadron target and also to plan future experiments.

In this work, we study quark and gluon GPDs of heavy nuclei and DVCS on nuclear targets at small values of Bjorken x_B (large energies). In particular, we generalize the theory of leading twist nuclear shadowing [11–13] to the case of GPDs and compute next-to-leading order quark and gluon GPDs of nuclei for $10^{-5} \leqslant x_B \leqslant 0.2$ and at a fixed virtuality Q^2. Using the obtained nuclear GPDs, we compute the DVCS amplitude, the DVCS cross section, and the DVCS beam-spin asymmetry for the heavy nuclear target of ^{208}Pb. Our results can be summarized as follows:

(i) Leading twist nuclear shadowing suppresses very significantly the DVCS amplitude and the DVCS cross section at small values of Bjorken x_B.

(ii) In the $\xi \to 0$ limit, nuclear GPDs reduce to impact-parameter-dependent nuclear parton distribution functions (PDFs). Therefore, nuclear GPDs allow one to access the spatial image of nuclear shadowing. The shadowing correction to nuclear GPDs introduces nontrivial correlations between the light-cone fraction x and the impact parameter b.

(iii) DVCS interferes with the purely electromagnetic Bethe-Heitler (BH) process. At small values of the momentum transfer t, which dominate coherent nuclear DVCS (without nuclear breakup), and also for the t-integrated cross sections, the BH cross section is much larger than the DVCS one. This makes it rather challenging to extract a small DVCS signal on the background of the dominant BH contribution to the $eA \to e\gamma A$ cross section. However, owing to the rapid t dependence, the DVCS cross section becomes (much) larger than the BH cross section near the minima of the nuclear form factor. This suggests that the measurements of nuclear DVCS at the values of t close

*Klaus.Goeke@tp2.rub.de
†vguzey@jlab.org
‡marat.siddikov@tp2.rub.de

to the minima of the nuclear form factor will not only be very sensitive to the magnitude of nuclear shadowing (owing to the suppression of the nonshadowed Born contribution) but will also have a sufficiently small BH contribution.

(iv) Another possible way to access nuclear GPDs in the small x_B region is through the measurement of the DVCS beam-spin asymmetry, A_{LU}. Nuclear shadowing causes dramatic oscillations of the asymmetry at fixed $\phi = 90^\circ$ as a function of the momentum transfer t. The position of the points where A_{LU} changes sign is directly related to the magnitude of nuclear shadowing.

The rest of the paper is structured as follows. In Sec. II we derive the expression for nuclear shadowing for nuclear GPDs. In Sec. III, we analyze the $\xi_A \to 0$ limit of the resulting nuclear GPDs, point out the equivalence of the nuclear GPDs in this limit to the impact-parameter-dependent nuclear PDFs, and discuss the spacial image of nuclear shadowing. Predictions for DVCS observables (the DVCS amplitude and cross section and the beam-spin DVCS asymmetry) are presented and discussed in Sec. IV. Finally, we summarize and draw conclusions in Sec. V.

II. LEADING TWIST NUCLEAR SHADOWING AND NUCLEAR GPDs

The nuclear structure function $F_{2A}(x_B, Q^2)$ measured in inclusive deep inelastic scattering (DIS) with nuclear targets differs from the sum of free nucleon structure functions $F_{2N}(x_B, Q^2)$ over the entire range of values of Bjorken x_B [14–17]. In particular, for small values of x_B, $10^{-5} \leqslant x_B \leqslant 0.05$–$0.1$, $F_{2A}(x_B, Q^2)/[AF_{2N}(x_B, Q^2)] < 1$, which is called *nuclear shadowing*.

As we learned from DIS with fixed nuclear targets, the effect of nuclear shadowing is quite large for small x_B. The kinematics of the future high-energy collider [18,19] will cover the small-x_B region, where the effect of nuclear shadowing will play a major role.

The leading twist theory of nuclear shadowing [11–13] is an approach to nuclear shadowing, in which nuclear shadowing in DIS with nuclei is explained in terms of hard diffraction in lepton-nucleon DIS. In particular, by using the QCD factorization theorems for inclusive and hard diffractive DIS and generalizing the result for nuclear shadowing in pion-deuteron scattering obtained by Gribov [20], the leading twist theory of nuclear shadowing makes predictions for the shadowing correction to nuclear PDFs, $\delta f_{j/A}(x_B, Q^2) \equiv f_{j/A}(x_B, Q^2) - Af_{j/N}(x_B, Q^2)$, in terms of the free nucleon (proton) diffractive PDFs $f_{j/N}^{D(4)}$ for small values of x_B, $10^{-5} \leqslant x_B \leqslant 0.2$. One should note that the generalization of Gribov's result to DIS and to nuclei heavier than deuterium makes an explicit assumption that the diffractive state produced in the interaction with the first nucleon of the target elastically rescatters off the rest of the nucleons (quasi-eikonal approximation) [11–13]. In the limit of low nuclear density, when the interaction with only two nucleons of the target is important, the relation between $\delta f_{j/A}(x_B, Q^2)$ and $f_{j/N}^{D(4)}$ is model independent. Since $f_{j/N}^{D(4)}$ is a leading twist quantity, so is $\delta f_{j/A}(x_B, Q^2)$, which explains the name *leading twist* theory of nuclear shadowing.

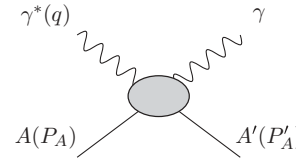

FIG. 1. DVCS on a nuclear target.

In this work, we generalize the theory of leading twist nuclear shadowing of usual nuclear PDFs [11–13] to the off-forward kinematics, DVCS on nuclear targets, and nuclear GPDs. The DVCS amplitude on any hadronic target is defined as a matrix element of the T-product of two electromagnetic currents (see, e.g., Ref. [3]),

$$H_A^{\mu\nu} = -i \int d^4x e^{-i\,q\cdot x} \langle P'_A | T\{J^\mu(x) J^\nu(0)\} | P_A \rangle, \qquad (1)$$

where $q(-q^2 = Q^2)$ is the momentum of the virtual photon and P_A and P'_A are the momenta of the initial and final nucleus, respectively. DVCS on a nuclear target is presented in Fig. 1.

For the analysis of the matrix element in Eq. (1), it is convenient to introduce two lightlike vectors $\tilde{p} = 1/\sqrt{2}(1, 0, 0, 1)$ and $n = 1/\sqrt{2}(1, 0, 0, -1)$ and to work in the so-called symmetric frame, where q and the average momentum of the initial and final nucleus, $\bar{P}_A \equiv (P_A + P'_A)/2$, are large and have no transverse component (with respect to the lightlike directions defined by $\tilde{p}$ and n). Then, the involved momenta can be parameterized as [3]

$$\begin{aligned} P_A &= (1+\xi_A)\bar{P}_A^+ \tilde{p} + \frac{\bar{M}_A^2}{2\bar{P}_A^+}(1-\xi_A)n - \frac{\vec{\Delta}_\perp}{2}, \\ P'_A &= (1-\xi_A)\bar{P}_A^+ \tilde{p} + \frac{\bar{M}_A^2}{2\bar{P}_A^+}(1+\xi_A)n + \frac{\vec{\Delta}_\perp}{2}, \\ \Delta &\equiv P'_A - P_A = -2\xi_A \bar{P}_A^+ \tilde{p} + \xi_A \frac{\bar{M}_A^2}{\bar{P}_A^+} n + \vec{\Delta}_\perp, \\ q &= -2\xi_A \bar{P}_A^+ \tilde{p} + \frac{Q^2}{4\xi_A \bar{P}_A^+} n, \end{aligned} \qquad (2)$$

where $\bar{P}_A^+ \equiv \bar{P}_A \cdot n$; $\bar{M}_A^2 = M_A^2 - t/4$, with M_A the mass of the nucleus and $t = \Delta^2$ the momentum transfer squared; Q^2 is the photon virtuality; $\vec{\Delta}_\perp$ is the component of Δ orthogonal to the vectors $\tilde{p}$ and n. As follows from the decomposition of Eq. (2),

$$\xi_A = \frac{Q^2}{4\,\bar{P}_A \cdot q} \approx \frac{x_A}{2 - x_A}, \qquad (3)$$

where x_A is the Bjorken variable with respect to the nuclear target,

$$x_A = \frac{Q^2}{2P_A \cdot q} = \frac{1}{A} x_B. \qquad (4)$$

The Bjorken variable x_B is defined in the usual way with respect to a free nucleon.

In this work, we shall consider spinless nuclei since we are not concerned with spin effects in nuclear shadowing.

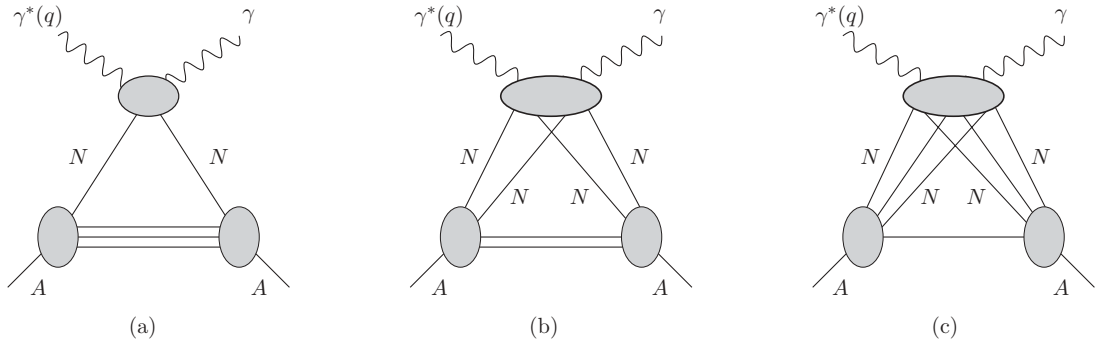

FIG. 2. Feynman graphs corresponding to the DVCS amplitude on a nuclear target, $H_A^{\mu\nu}$, showing the impulse (Born) approximation (a) and the shadowing correction arising from the interaction with two nucleons (b) and three nucleons of the target (c), respectively.

To the leading twist accuracy and to the leading order in the strong coupling constant, $H_A^{\mu\nu}$ of a spinless nucleus is expressed in terms of a single generalized parton distribution, H_A, convoluted with the hard scattering coefficient function $C^+(x,\xi_A)$, (see, e.g., Ref. [3]),

$$H_A^{\mu\nu} = -g_\perp^{\mu\nu}\int_{-1}^{1} dx\, C^+(x,\xi_A) H_A(x,\xi_A,t,Q^2) \equiv -g_\perp^{\mu\nu}\,\mathcal{H}_A(\xi_A,t,Q^2), \tag{5}$$

where $g_\perp^{\mu\nu} = g^{\mu\nu} - \tilde{p}^\mu n^\nu - \tilde{p}^\nu n^\mu$ and $C^+(x,\xi_A) = 1/(x - \xi_A + i\epsilon) + 1/(x + \xi_A - i\epsilon)$. The function $\mathcal{H}_A$ is also called the Compton form factor (CFF).

At sufficiently high energies (small Bjorken x_B), the virtual photon interacts with many (all) nucleons of the target and the DVCS amplitude on a nuclear target, $H_A^{\mu\nu}$, receives contributions from the graphs presented in Fig. 2. Figures 2(a), 2(b), and 2(c) correspond to the interaction with one, two, and three nucleons, respectively. Graphs that correspond to the interaction with four and more nucleons of the target are not shown, but they are implied. Therefore, $H_A^{\mu\nu}$ can be written as the following sum:

$$H_A^{\mu\nu} = H_A^{(a)\mu\nu} + H_A^{(b)\mu\nu} + H_A^{(c)\mu\nu} + \cdots, \tag{6}$$

where the terms in the right-hand side correspond to the graphs shown in Figs. 2(a), 2(b), and 2(c), respectively.

A. Impulse approximation

Let us start with the calculation of the graph shown in Fig. 2(a). For the case of a deuterium target, the derivation was done in Ref. [21]. Therefore, in this section, we shall follow Ref. [21], making straightforward generalizations to heavier nuclei and high-energy kinematics. The calculation of the graph in Fig. 2(a) can be carried out straightforwardly using the light-cone (LC) formalism. In this formalism, each state is characterized by its plus-momentum $p^+ = p\cdot n = (p^0 + p^3)/\sqrt{2}$, the transverse momentum $\vec{p}_\perp$, and the helicity λ. The minimal Fock component of the nuclear state $|P_A\rangle$ is expressed in terms of the nuclear LC wave function ϕ_A and the product of nucleon states as

$$|P_A^+, \vec{P}_{\perp A}\rangle = \sum_{\lambda_i}\int\prod_{i=1}^{A}\frac{d\alpha_i}{\sqrt{\alpha_i}}\frac{d^2\vec{k}_{\perp i}}{16\pi^3}\,16\pi^3\,\delta\left(\sum_{j=1}^{A}\alpha_j - 1\right)\delta\left(\sum_{j=1}^{A}\vec{k}_{\perp j}\right) \times \phi_A(\alpha_1,\vec{k}_{\perp 1},\lambda_1,\alpha_2,\vec{k}_{\perp 2},\lambda_2,\ldots) \times |\alpha_i P_A^+, \vec{k}_{\perp i} + \alpha_i\vec{P}_{\perp A},\lambda_i\rangle, \tag{7}$$

where $\alpha_i = p_i^+/P_A^+$ is the fraction of the nucleus plus-momentum carried by nucleon i. Since we are not concerned with the correlations of nucleons in the target nucleus, we take ϕ_A as a product of the LC wave functions of individual nucleons, ϕ_N,

$$\phi_A(\alpha_1,\vec{k}_{\perp 1},\lambda_1,\alpha_2,\vec{k}_{\perp 2},\lambda_2,\ldots) = \prod_{i=1}^{A}\phi_N(\alpha_i,\vec{k}_{\perp i},\lambda_i). \tag{8}$$

Substituting Eq. (7) for the initial and final nuclear states in the nuclear DVCS amplitude [Eq. (5)], we obtain

$$H_A^{(a)\mu\nu} = -i\int d^4x e^{-i\,q\cdot x}\sum_N\sum_\lambda\int\frac{d\alpha}{\sqrt{\alpha\,\alpha'}}\frac{d^2\vec{k}_\perp}{16\pi^3} \times \rho_A^N(\alpha',\vec{k}'_\perp,\lambda|\alpha,\vec{k}'_\perp,\lambda) \times \langle p'_N|T\{J^\mu(x)J^\nu(0)\}|p_N\rangle, \tag{9}$$

where $\sum_N$ denotes the sum over active (interacting) nucleons. In Eq. (9) and in the rest of the paper, we neglect the off-shellness of the nucleons in the photon-nucleon scattering amplitude, which is a small correction of $\mathcal{O}(\epsilon/m_N)$, where ϵ is the average nuclear binding energy and m_N is the mass of the nucleon. The effect of the off-shellness in nuclear DVCS was considered and estimated in Refs. [22,23].

The initial and final states of the active nucleon are

$$|p_N\rangle = \left|\alpha(1+\xi_A)\bar{P}_A^+, \vec{k}_\perp - \alpha\frac{\vec{\Delta}_\perp}{2},\lambda\right\rangle, \qquad |p'_N\rangle = \left|\alpha'(1-\xi_A)\bar{P}_A^+, \vec{k}'_\perp + \alpha'\frac{\vec{\Delta}_\perp}{2},\lambda\right\rangle. \tag{10}$$

The LC fraction and the transverse momentum of the active nucleon are found from the conservation of the LC

energy-momentum in the elementary $\gamma^* N \to \gamma N$ vertex:

$$\alpha' = \frac{1+\xi_A}{1-\xi_A}\alpha - \frac{2\xi_A}{1-\xi_A} \approx \alpha - 2\xi_A,$$
$$\vec{k}'_\perp = \vec{k}_\perp + \frac{1-\alpha}{1-\xi_A}\vec{\Delta}_\perp \approx \vec{k}_\perp + (1-\alpha)\vec{\Delta}_\perp. \quad (11)$$

In these equations, the approximate relations hold after one neglects ξ_A compared to unity.

The function ρ_A^N is the overlap between the initial and final nuclear LC wave functions,

$$\rho_A^N(\alpha', \vec{k}'_\perp, \lambda|\alpha, \vec{k}_\perp, \lambda)$$
$$= \left(\sqrt{\frac{1+\xi_A}{1-\xi_A}}\right)^{A-1} \phi_N^*(\alpha', \vec{k}'_\perp, \lambda)\phi_N(\alpha, \vec{k}_\perp, \lambda)$$
$$\times \sum_{\lambda_i}\int \prod_{i=2}^{A} \frac{d\alpha_i\, d^2\vec{k}_{\perp i}}{16\pi^3}\delta\left(\alpha + \sum_{j=2}^{A}\alpha_j - 1\right)$$
$$\times 16\pi^3\delta\left(\vec{k}_\perp + \sum_{j=2}^{A}\vec{k}_{\perp j}\right)|\phi_N(\alpha_i, \vec{k}_{\perp i}, \lambda_i)|^2$$
$$\approx \phi_N^*(\alpha', \vec{k}'_\perp, \lambda)\phi_N(\alpha, \vec{k}_\perp, \lambda). \quad (12)$$

The last line is an approximation valid for sufficiently large nuclei, when the effects associated with the motion of the center of mass of the nucleus (taken into account by the δ functions) can be safely neglected. Note that helicity conservation requires that the helicity of the active nucleon be the same in the initial and in the final state.

The matrix element in Eq. (9) can be evaluated by making a transverse boost to the symmetric frame of the active nucleon [21]. In that frame, one can use the standard definition,

$$-i\int d^4x e^{-i\,q\cdot x}\langle p'_N|T\{J^\mu(x)J^\nu(0)\}|p_N\rangle$$
$$= H_N^{\mu\nu}(\xi_N, t, Q^2), \quad (13)$$

where $H_N^{\mu\nu}$ is the DVCS amplitude for the bound nucleon. The skewedness ξ_N is determined with the respect to the active nucleon,

$$\xi_N \equiv \frac{Q^2}{4\bar{p}_N\cdot q} = \frac{\xi_A}{(1+\xi_A)\alpha - \xi_A}, \quad (14)$$

where $\bar{p}_N = (p_N + p'_N)/2$. Therefore, we obtain the connection between the DVCS amplitudes for the nuclear target and for the bound nucleon,

$$H_A^{(a)\mu\nu} = \sum_N\sum_\lambda\int \frac{d\alpha}{\sqrt{\alpha\,\alpha'}}\frac{d^2\vec{k}_\perp}{16\pi^3}\,\rho_A^N(\alpha', \vec{k}'_\perp, \lambda|\alpha, \vec{k}_\perp, \lambda)$$
$$\times H_N^{\mu\nu}(\xi_N, t, Q^2). \quad (15)$$

To the leading twist accuracy, the DVCS amplitude for the bound nucleon is parametrized in terms of four nucleon GPDs, H_N, E_N, $\tilde{H}_N$ and $\tilde{E}_N$:

$$H_N^{\mu\nu}(\xi_N, t, Q^2)$$
$$= \frac{1}{2\bar{p}_N^+}(-\tilde{g}_\perp^{\mu\nu})\int_{-1}^{1} dx C^+(x, \xi_N)$$
$$\times \left[H_N(x, \xi_N, t)\bar{u}(p'_N)\gamma^+ u(p_N)\right.$$
$$\left. + E_N(x, \xi_N, t)\bar{u}(p'_N)\frac{i\sigma^{+\lambda}\Delta_\lambda}{2m_N}u(p_N)\right] + \cdots, \quad (16)$$

where $\cdots$ denotes the contribution of the GPDs $\tilde{H}_N$ and $\tilde{E}_N$. The tensor $\tilde{g}_\perp^{\mu\nu}$ is defined in the boosted frame (the symmetric frame of the active nucleon) and, to a good accuracy, is equal to $g_\perp^{\mu\nu}$ entering Eq. (5),

$$\tilde{g}_\perp^{\mu\nu} \equiv g^{\mu\nu} - \frac{\tilde{q}^\mu\tilde{\bar{p}}_N^\nu + \tilde{q}^\nu\tilde{\bar{p}}_N^\mu}{\tilde{q}\cdot\tilde{\bar{p}}_N} + \frac{\tilde{q}^\mu\tilde{q}^\nu}{(\tilde{q}\cdot\tilde{\bar{p}}_N)^2}\tilde{\bar{p}}_N^2 + \frac{\tilde{\bar{p}}_N^\mu\tilde{q}^\nu}{(\tilde{\bar{p}}_N\cdot\tilde{\bar{p}}_N)^2}q^2$$
$$\approx g^{\mu\nu} - \tilde{p}^\mu n^\nu - \tilde{p}^\nu n^\mu + \mathcal{O}\left(\frac{x_B^2\bar{m}_N^2}{Q^2}, \frac{1}{Q^2R_A^2}\right), \quad (17)$$

where the vectors $\tilde{q}$ and $\tilde{\bar{p}}_N$ refer to the boosted frame, $\bar{m}_N^2 = m_N^2 - t/4$, and R_A is the nuclear radius. In the derivation of Eq. (17) we used the fact that the transverse boost to the symmetric frame of the active nucleon has not changed the plus-component of the vectors and that the typical (transverse) momenta of nucleons in a nucleus, $|\vec{p}_{N\perp}| \sim 1/R_A$, are small compared to the virtuality Q^2.

Using the fact that the helicities of the bound nucleon in the initial and final states are the same and making a natural assumption that ρ_A^N is the same for the $\lambda = \pm 1$ helicities, we observe that the nucleon GPDs $\tilde{H}$ and $\tilde{E}$ do not contribute to Eq. (15), which is a consequence of the LC spinor algebra (see, e.g., Ref. [21]). In addition, since we are interested in the kinematics, where the values of x_B and ξ_N are small, the contribution of the GPDs E, which enters Eq. (15) with the prefactor ξ_N^2, can be safely neglected. Therefore, we have that the DVCS amplitude for the bound nucleon reads (keeping in mind the equal helicities of the initial and final nucleon)

$$H_N^{\mu\nu}(\xi_N, t, Q^2) = -g_\perp^{\mu\nu}\sqrt{1-\xi_N^2}\,\mathcal{H}_N(\xi_N, t, Q^2)$$
$$\approx -g_\perp^{\mu\nu}\mathcal{H}_N(\xi_N, t, Q^2), \quad (18)$$

where $\mathcal{H}_N$ is the CFF of the bound nucleon. Thus, we obtain our final relation between the CFFs of the nuclear target in the impulse approximation, $\mathcal{H}_A^{(a)}$, and that of the bound nucleon,

$$\mathcal{H}_A^{(a)}(\xi_A, t, Q^2)$$
$$= \sum_N\sum_\lambda\int \frac{d\alpha}{\sqrt{\alpha\,\alpha'}}\frac{d^2\vec{k}_\perp}{16\pi^3}\rho_A^N(\alpha', \vec{k}'_\perp, \lambda|\alpha, \vec{k}_\perp, \lambda)$$
$$\times \mathcal{H}_N(\xi_N, t, Q^2). \quad (19)$$

It is important to point out that the integration over α (longitudinal convolution) and $\vec{k}_\perp$ (transverse convolution) takes into account the effect of the motion of the bound nucleons in the target (Fermi motion effect). The Fermi motion effect in DVCS on nuclear targets in the form of longitudinal convolution was also considered in Refs. [21,24–27]. Both the longitudinal and transverse convolutions along with the modifications of the bound-nucleon GPDs, which depend on $\vec{k}_\perp$, were considered in Refs. [22,23].

To interpret the function ρ_A^N and to fix its normalization, it is useful to consider the electromagnetic form factor of a spin-0 nucleus, $F_A^{\rm em}$, which is defined as the matrix element of

the operator of the electromagnetic current,

$$\langle P'_A|J^\mu(0)|P_A\rangle = 2\bar{P}^\mu_A F^{\rm em}_A(t). \tag{20}$$

Using the LC formalism just presented, we consider the plus-component of Eq. (20) and obtain

$$2\bar{P}^+_A F^{\rm em}_A(t) = \sum_N \sum_\lambda \int \frac{d\alpha}{\sqrt{\alpha\,\alpha'}} \frac{d^2\vec{k}_\perp}{16\pi^3} \rho^N_A(\alpha', \vec{k}'_\perp, \lambda|\alpha, \vec{k}_\perp, \lambda) \times \langle p'_N|J^+(0)|p_N\rangle. \tag{21}$$

In the reference frame in which we work, the momentum transfer Δ is predominantly transverse at small x_B [see Eq. (2)]. Therefore, the nucleon matrix element for the same nucleon helicities is (predominantly) proportional to the Dirac nucleon form factor, $F_{1N}(t)$:

$$\langle p'_N|J^+(0)|p_N\rangle \approx \bar{u}(p'_N)\gamma^+ u(p_N) F_{1N}(t) \approx 2\bar{p}^+_N F_{1N}(t) = 2\,\frac{\xi_A}{\xi_N}\,\bar{P}^+_A\,F_{1N}(t). \tag{22}$$

Therefore,

$$\begin{aligned} F^{\rm em}_A(t) &= \sum_N F_{1N}(t) \frac{\xi_A}{\xi_N} \sum_\lambda \int \frac{d\alpha}{\sqrt{\alpha\alpha'}} \frac{d^2\vec{k}_\perp}{16\pi^3} \rho^N_A(\alpha', \vec{k}'_\perp, \lambda|\alpha, \vec{k}_\perp, \lambda) \\ &= \sum_N F_A(t)\, F_{1N}(t), \end{aligned} \tag{23}$$

where we have introduced the nuclear form factor associated with the distribution of nucleons in the nucleus (associated with the nuclear density),

$$F_A(t) \equiv \frac{\xi_A}{\xi_N} \int \frac{d\alpha}{\sqrt{\alpha\alpha'}} \frac{d^2\vec{k}_\perp}{16\pi^3} \rho^N_A(\alpha', \vec{k}'_\perp, \lambda|\alpha, \vec{k}_\perp, \lambda). \tag{24}$$

As follows from Eq. (23), $F_A(t)$ is normalized to unity [$F_A(0) = 1$]. This condition also fixes the normalization of the nuclear LC wave function,

$$\sum_\lambda \int \frac{d\alpha}{\alpha} \frac{d^2\vec{k}_\perp}{16\pi^3} \rho^N_A(\alpha, \vec{k}_\perp, \lambda|\alpha, \vec{k}_\perp, \lambda) = \sum_\lambda \int \frac{d\alpha}{\alpha} \frac{d^2\vec{k}_\perp}{16\pi^3} |\phi^N(\alpha, \vec{k}_\perp, \lambda)|^2 = A. \tag{25}$$

At small x_B, the effect of the Fermi motion can be safely neglected (see, e.g., Ref. [28]), and, as a consequence, Eq. (19) can be significantly simplified as follows. The function ρ^N_A is peaked around $\alpha \approx 1/A$. Thus, if one neglects the Fermi motion of the bound nucleon, one evaluates ξ_N at $\alpha = 1/A$ (where, for brevity, we shall use the same notation), obtaining

$$\xi_N \equiv \xi_N(\alpha = 1/A) = \frac{\xi_A}{\frac{1}{A}(1+\xi_A) - \xi_A} \approx A\,\xi_A. \tag{26}$$

Therefore, by neglecting the Fermi motion and using Eq. (24), Eq. (19) can be written in the following simplified and approximate form:

$$\mathcal{H}^{(a)}_A(\xi_A, t, Q^2) = \frac{\xi_N}{\xi_A} \sum_N F_A(t)\, \mathcal{H}_N(\xi_N, t, Q^2). \tag{27}$$

As a number of nucleons, $\mathcal{H}^{(a)}_A$ scales as A^2, which is a natural scaling of the nuclear CFF [29]. The inclusion of the Fermi motion effect and the effect associated with non-nucleon degrees of the freedom in the nucleus modifies this intuitive scaling [27,30].

The next important step is the conversion of the relation between nucleus and nucleon CFFs [Eq. (27)] into a similar relation between the corresponding GPDs. To the leading twist accuracy and to the leading order in the strong coupling constant,

$$\begin{aligned} \mathcal{H}_A(\xi_A, t) &= \int_{-1}^{1} dx\, H_A(x, \xi_A, t) \times \left(\frac{1}{x - \xi_A + i\epsilon} + \frac{1}{x + \xi_A - i\epsilon}\right), \\ \mathcal{H}_N(\xi_N, t) &= \int_{-1}^{1} dx_N\, H_N(x_N, \xi_N, t) \times \left(\frac{1}{x_N - \xi_N + i\epsilon} + \frac{1}{x_N + \xi_N - i\epsilon}\right). \end{aligned} \tag{28}$$

The relevant quark LC fractions and momenta of the active nucleon and the target nucleus are presented in Fig. 3. Figure 3(a) represents the generic handbag approximation for DVCS on a nuclear target, which expresses the CFF $\mathcal{H}_A$ in terms of the nuclear GPD H_A and which corresponds to the first line of Eq. (28).

At the same time, $\mathcal{H}^{(a)}_A$ can be expressed in terms of the nucleon CFF $\mathcal{H}_N$ [see Eq. (27) and Fig. 3(b)]. In this case, the nucleon GPD depends on the LC fractions ξ_N defined by Eq. (14) and on x_N, which is defined with respect to the active nucleon,

$$x_N \equiv \frac{\bar{k}\cdot n}{\bar{p}_N \cdot n} = \frac{x}{\alpha(1+\xi_A) - \xi_A}, \tag{29}$$

where $\bar{k} = (k + k')/2$ and k and k' are the momenta of the initial and final lepton, respectively. A useful consequence of Eq. (29) is the proportionality of the LC fractions x_N and x:

$$\frac{x_N}{\xi_N} = \frac{x}{\xi_A}. \tag{30}$$

This relation allows us to find the LC fractions of the interacting quark in Fig. 3(b), which are equal to $x + \xi_A = (\xi_A/\xi_N)(x_N + \xi_N)$ and $x - \xi_A = (\xi_A/\xi_N)(x_N - \xi_N)$, respectively. Since the absolute value of x_N cannot exceed unity, we find that

$$|x| \leqslant \frac{\xi_A}{\xi_N} \approx \frac{1}{A}. \tag{31}$$

Note that the limit $|x| \leqslant 1/A$ is standard for the approximation, when the nucleus consists of A stationary nucleons. Using

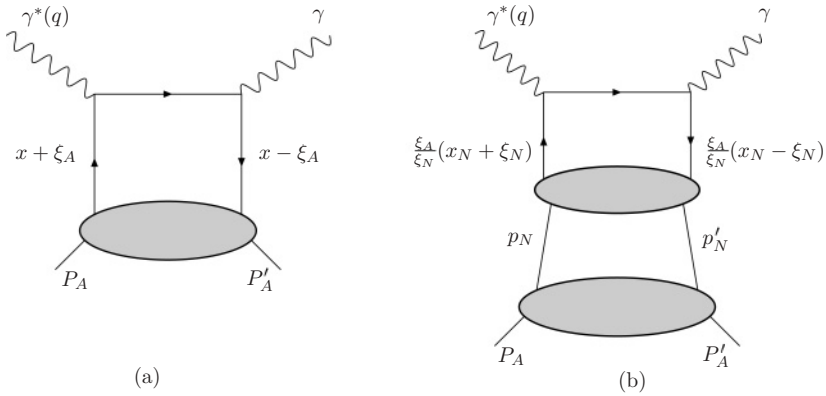

FIG. 3. The handbag mechanism for DVCS on a nuclear target. (a) The generic representation of nuclear GPDs. (b) A more detailed representation of the same quantity in terms of bound-nucleon GPDs. Shown are relevant quark light-cone fractions and momenta of the active nucleon and the target nucleus.

Eq. (19) and the second line of Eq. (28), we obtain

$$\begin{aligned}
&\mathcal{H}_A^{(a)}(\xi_A, t, Q^2) \\
&= \sum_N \sum_\lambda \int \frac{d\alpha}{\sqrt{\alpha\,\alpha'}} \frac{d^2\vec{k}_\perp}{16\pi^3}\, \rho_A^N(\alpha', \vec{k}'_\perp, \lambda | \alpha, \vec{k}_\perp, \lambda) \\
&\quad \times \int_{-1}^{1} dx_N\, H_N(x_N, \xi_N, t) \\
&\quad \times \left(\frac{1}{x_N - \xi_N + i\epsilon} + \frac{1}{x_N + \xi_N - i\epsilon} \right) \\
&= \sum_N \sum_\lambda \int \frac{d\alpha}{\sqrt{\alpha\,\alpha'}} \frac{d^2\vec{k}_\perp}{16\pi^3}\, \rho_A^N(\alpha', \vec{k}'_\perp, \lambda | \alpha, \vec{k}_\perp, \lambda) \\
&\quad \times \int_{-\xi_A/\xi_N}^{\xi_A/\xi_N} dx\, H_N(x_N, \xi_N, t) \\
&\quad \times \left(\frac{1}{x - \xi_A + i\epsilon} + \frac{1}{x + \xi_A - i\epsilon} \right). \qquad (32)
\end{aligned}$$

Recalling the first line of Eq. (28) and the limits of integration over x [Eq. (31)], we obtain the desired relation between the nuclear GPD in the impulse approximation, $H_A^{(a)}$, and the nucleon GPD:

$$\begin{aligned}
&H_A^{(a)}(\xi_A, t, Q^2) \\
&= \sum_N \sum_\lambda \int \frac{d\alpha}{\sqrt{\alpha\,\alpha'}} \frac{d^2\vec{k}_\perp}{16\pi^3}\, \rho_A^N(\alpha', \vec{k}'_\perp, \lambda | \alpha, \vec{k}_\perp, \lambda) \\
&\quad \times H_N(x_N, \xi_N, t, Q^2). \qquad (33)
\end{aligned}$$

We would like to note that Eq. (33) could also be derived by starting directly from the definition of the nuclear GPD as the matrix element between nuclear states and applying the LC formalism for the nuclear states, as we did for the DVCS amplitude.

Equation (33) is derived for the nuclear (nucleon) GPDs, which are sums of quark GPDs weighted with the quark electric charge squared. Certainly, the relation between the nuclear and nucleon GPDs holds for individual parton flavors (quarks and gluons):

$$\begin{aligned}
&H_A^{j(a)}(\xi_A, t, Q^2) \\
&= \sum_N \sum_\lambda \int \frac{d\alpha}{\sqrt{\alpha\,\alpha'}} \frac{d^2\vec{k}_\perp}{16\pi^3}\, \rho_A^N(\alpha', \vec{k}'_\perp, \lambda | \alpha, \vec{k}_\perp, \lambda) \\
&\quad \times H_N^j(x_N, \xi_N, t, Q^2), \qquad (34)
\end{aligned}$$

where j is the parton flavor.

As we have already explained, the Fermi motion effect can be safely neglected at large energies [see Eq. (27)]. In this case, Eq. (34) can be simplified and written in the following form:

$$H_A^{j(a)}(x, \xi_A, t, Q^2) \approx \frac{\xi_N}{\xi_A} \sum_N F_A(t)\, H_N^j(x_N, \xi_N, t, Q^2). \qquad (35)$$

B. Double scattering correction

The graph in Fig. 2(b) describes the contribution to DVCS on a nuclear target, when the interaction involves two nucleons of the target. This graph gives the leading contribution to nuclear shadowing. Details of the kinematics of the graph in Fig. 2(b) are presented in Fig. 4.

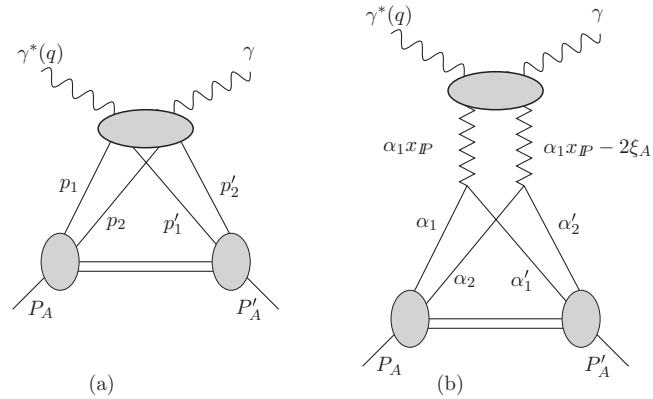

FIG. 4. Double rescattering correction to DVCS on a nuclear target. (a) The shadowing correction in terms of the $\gamma^* NN \to \gamma NN$ amplitude. (b) An approximation based on the assumption that the shadowing correction can be expressed in terms of DVCS on a Pomeron, $\gamma^* I\!P \to \gamma I\!P$. Also shown are the relevant light-cone momentum fractions.

Using the LC formalism, we obtain the following expression for the contribution of the graph in Fig. 2(b):

$$
\begin{aligned}
&H_A^{(b)\mu\nu} \\
&= -i\int d^4x\, e^{-iq\cdot x}\sum_{\text{pairs}}\int\frac{d\alpha_1'}{\sqrt{\alpha_1'\alpha_2'}}\frac{d^2\vec{k}_{\perp 1}'}{16\pi^3}\frac{d\alpha_1 d\alpha_2}{\sqrt{\alpha_1\alpha_2}}\frac{d^2\vec{k}_{\perp 1}d^2\vec{k}_{\perp 2}}{(16\pi^3)^2} \\
&\quad\times\rho_A^{2N}(\alpha_1'\alpha_2',\vec{k}_{\perp 1}',\vec{k}_{\perp 2}'|\alpha_1,\alpha_2,\vec{k}_{\perp 1},\vec{k}_{\perp 2}) \\
&\quad\times\langle p_1'p_2'|T\{J^\mu(x)J^\nu(0)\}|p_1p_2\rangle,
\end{aligned}
\tag{36}
$$

where $\sum_{\text{pairs}}$ denotes the sum over the pairs of the active nucleons with momenta p_1 and p_2 in the initial state and with momenta p_1' and p_2' in the final state. Each state is characterized by the corresponding LC fractions and transverse momenta:

$$
\begin{aligned}
|p_{1,2}\rangle &= \left|\alpha_{1,2}(1+\xi_A)\bar{P}_A^+,\vec{k}_{\perp 1,2}-\alpha_{1,2}\frac{\vec{\Delta}_\perp}{2}\right\rangle, \\
|p_{1,2}'\rangle &= \left|\alpha_{1,2}'(1-\xi_A)\bar{P}_A^+,\vec{k}_{\perp 1,2}'+\alpha_{1,2}'\frac{\vec{\Delta}_\perp}{2}\right\rangle.
\end{aligned}
\tag{37}
$$

The LC fractions and the transverse momenta of the active nucleons are related by the conservation of the LC energy-momentum [see also Eq. (11)]:

$$
\begin{aligned}
\alpha_1'+\alpha_2' &= \alpha_1+\alpha_2-2\xi_A, \\
\vec{k}_{\perp 1}'+\vec{k}_{\perp 2}' &= \vec{k}_{\perp 1}+\vec{k}_{\perp 2}+\vec{\Delta}_\perp,
\end{aligned}
\tag{38}
$$

where we have neglected the factors ξ_A and $\alpha_{1,2}$ compared to unity.

For brevity, we shall not show explicitly the nucleon helicities, keeping in mind that the interaction does not change the helicity of the nucleons. The function ρ_A^{2N} is given by the following overlap of the nuclear LC wave functions:

$$
\begin{aligned}
&\rho_A^{2N}(\alpha_1'\alpha_2',\vec{k}_{\perp 1}',\vec{k}_{\perp 2}'|\alpha_1,\alpha_2,\vec{k}_{\perp 1},\vec{k}_{\perp 2}) \\
&\quad=\phi_N^*(\alpha_1',\vec{k}_{\perp 1}')\phi_N(\alpha_1,\vec{k}_{\perp 1})\phi_N^*(\alpha_2',\vec{k}_{\perp 2}')\phi_N(\alpha_2,\vec{k}_{\perp 2}) \\
&\qquad\times\int\prod_{i=3}^{A}\frac{d\alpha_i\,d^2\vec{k}_{\perp i}}{16\pi^3}\delta\left(\sum_{j=1}^{A}\alpha_j-1\right) \\
&\qquad\times 16\pi^3\delta\left(\sum_{j=1}^{A}\vec{k}_{\perp j}\right)|\phi_N(\alpha_i',\vec{k}_{\perp i}')|^2 \\
&\quad\approx\phi_N^*(\alpha_1',\vec{k}_{\perp 1}')\phi_N(\alpha_1,\vec{k}_{\perp 1})\phi_N^*(\alpha_2',\vec{k}_{\perp 2}')\phi_N(\alpha_2,\vec{k}_{\perp 2}).
\end{aligned}
\tag{39}
$$

Equation (36) is a general expression corresponding to the graph in Fig. 2(b) and to the graph in Fig. 4(a). To proceed with the derivation, we need to model the multiparticle matrix element $\langle p_1'p_2'|T\{J^\mu(x)J^\nu(0)\}|p_1p_2\rangle$. Our model for the $\langle p_1'p_2'|T\{J^\mu(x)J^\nu(0)\}|p_1p_2\rangle$ matrix element is based on the studies of hard inclusive diffraction in DIS on the proton at HERA in the reaction $ep\to eXp$ [31–34], which we shall briefly review in the following.

The diffractive DIS $ep\to eXp$ reaction is presented in Fig. 5. The $ep\to eXp$ cross section is expressed in terms

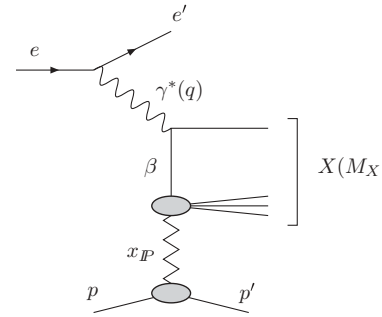

FIG. 5. Diffractive DIS on the proton.

of the diffractive structure functions $F_2^{D(4)}$ and $F_L^{D(4)}$ as

$$
\begin{aligned}
&\frac{d^4\sigma_{ep}^D}{dx_{I\!P}\,dt\,dx_B\,dQ^2} \\
&\quad=\frac{2\pi\alpha_{\text{em}}^2}{x_BQ^4}[(1+(1-y)^2)F_2^{D(4)}(x_B,Q^2,x_{I\!P},t) \\
&\quad-y^2F_L^{D(4)}(x_B,Q^2,x_{I\!P},t)],
\end{aligned}
\tag{40}
$$

where α_{em} is the fine-structure constant and $y=(p\cdot q)/(p\cdot k)$ is the fractional energy loss of the incoming lepton. The variables t, $x_{I\!P}$, and β are characteristic for diffractive processes,

$$
\begin{aligned}
t &= (p'-p)^2, \\
x_{I\!P} &= \frac{q\cdot(p-p')}{q\cdot p}\approx\frac{M_X^2+Q^2}{W^2+Q^2}, \\
\beta &= \frac{x}{x_{I\!P}}=\frac{Q^2}{2q\cdot(p-p')}\approx\frac{Q^2}{Q^2+M_X^2},
\end{aligned}
\tag{41}
$$

where M_X is the invariant mass of the diffractively produced final state and $W^2=(q+p)^2$. The variable $x_{I\!P}$ is the fraction of the proton LC momentum lost in the diffractive scattering (the LC fraction carried by the Pomeron); β is the LC momentum carried by the interacting quark (parton). As follows from the definition of $x_{I\!P}$, the minimal value of $x_{I\!P}$ is equal to Bjorken x_B, which corresponds to $M_X=0$. Typically, the contribution of $F_L^{D(4)}$ is neglected because of its smallness and because of the kinematic suppression by the y^2 factor.

One of the main physics results of HERA is the observation that hard diffraction in DIS constitutes a fairly large part (10%–15%) of all DIS events and that hard diffraction in DIS is a leading twist phenomenon, that is, that the diffractive structure function $F_2^{D(4)}$ approximately scales (i.e., it only weakly—logarithmically—depends on Q^2).

The factorization theorem for hard diffraction in DIS [35] states that, at given fixed t and $x_{I\!P}$, the diffractive structure function $F_2^{D(4)}$ can be written as a convolution of the hard scattering coefficient function C_j with the universal diffractive parton distributions $f_j^{D(4)}$ (where j is the parton flavor):

$$
\begin{aligned}
F_2^{D(4)}(x,Q^2,x_{I\!P},t) &= \frac{x}{x_{I\!P}}\sum_{j=q,\bar{q},g}\int_{x/x_{I\!P}}^1\frac{d\beta'}{\beta'}C_j\left(\frac{x}{x_{I\!P}\beta'},Q^2\right) \\
&\quad\times f_j^{D(4)}(\beta',Q^2,x_{I\!P},t).
\end{aligned}
\tag{42}
$$

It is a phenomenological observation, which follows from the QCD analysis of the HERA data on inclusive diffraction, that the diffractive PDFs $f_j^{D(4)}$ can be written as a product of the Pomeron flux $f_{I\!P/p}$, the parton distribution function of the Pomeron, $f_{j/I\!P}$, and the factor describing the t dependence,

$$f_j^{D(4)}(\beta, Q^2, x_{I\!P}, t) = f_{I\!P/p}(x_{I\!P}) f_{j/I\!P}(\beta, Q^2) B_{\rm diff}\, e^{B_{\rm diff} t}. \tag{43}$$

In Eq. (43), we neglected the contribution of the subleading (Reggeon) exchange, which is not important in the considered kinematics. The Pomeron flux has the following form [33,34]:

$$f_{I\!P/p}(x_{I\!P}) = \int_{-1\,{\rm GeV}^2}^{t_{\rm min}} dt\, A_{I\!P} \frac{e^{B_{I\!P} t}}{x_{I\!P}^{2\alpha_{I\!P}(t)-1}}, \qquad \alpha_{I\!P}(t) = \alpha_{I\!P}(0) + \alpha'_{I\!P} t, \tag{44}$$

where $t_{\rm min} \approx -m_N^2 x_B^2 \approx 0$, $B_{I\!P} = 5.5\,{\rm GeV}^{-2}$, $\alpha_{I\!P}(0) = 1.111$ (Fit B of Ref. [33]), and $\alpha'_{I\!P} = 0.06\,{\rm GeV}^{-2}$. The coefficient $A_{I\!P}$ is found from the condition $x_{I\!P} f_{I\!P/p}(x_{I\!P}) = 1$ at $x_{I\!P} = 0.003$.

The PDFs of the Pomeron, $f_{j/I\!P}$, are found from global fits to the HERA data on hard diffraction taken by the ZEUS and H1 experiments [31–34] using the QCD factorization theorem [Eq. (42)]. One of the main results of such fits is that the gluon diffractive PDFs is much larger than the quark diffractive PDFs.

The t dependence of hard inclusive diffraction at HERA was recently measured by the H1 Collaboration using the forward proton spectrometer, which allows the final proton to be detected [34]. In the kinematics of the experiment, the data were well described by the simple exponential form [Eq. (43)] with the slope $B_{\rm diff} \approx 6\,{\rm GeV}^{-2}$. (Note that $f_j^{D(4)}$ has the dimension ${\rm GeV}^{-2}$.)

Our model for the $\langle p_1' p_2' | T\{J^\mu(x) J^\nu(0)\} | p_1 p_2\rangle$ matrix element is based on the observation that, in the considered kinematics, the interaction of the active nucleons with the virtual and real photons has a diffractive character and, hence, proceeds via the t-channel exchange with the vacuum quantum numbers (i.e., the Pomeron). The model is schematically presented in Fig. 4(b). The space-time picture of the process is the following. Nucleon 1 with longitudinal momentum fraction α_1 emits a Pomeron with momentum fraction $\alpha_1 x_{I\!P}$. The virtual photon undergoes DVCS on that Pomeron, producing a real photon and a Pomeron with the LC fraction $\alpha_1 x_{I\!P} - 2\xi_A$, which is absorbed by nucleon 2. Note that although the skewedness ξ_A is fixed by the external kinematics, the variable $x_{I\!P}$ is integrated over since it is related to the LC fractions of the active nucleons,

$$\alpha_1' = \alpha_1 - \alpha_1 x_{I\!P}, \qquad \alpha_2' = \alpha_2 + \alpha_1 x_{I\!P} - 2\xi_A. \tag{45}$$

The variable $x_{I\!P}$ has a clear physical interpretation: It is the fraction of the LC momentum of the nucleon carried by the Pomeron (see the previous discussion of diffraction in DIS). Whereas $x_{I\!P}$ is the relevant variable for the Pomeron emitted by nucleon 1, for the Pomeron emitted by nucleon 2, the relevant fraction is

$$\frac{\alpha_2' - \alpha_2}{\alpha_2} = \frac{\alpha_1 x_{I\!P} - 2\xi_A}{\alpha_2} \approx x_{I\!P} - 2\xi_N. \tag{46}$$

Based on this discussion, our model for $\langle p_1' p_2' | T\{J^\mu(x) J^\nu(0)\} | p_1 p_2\rangle$ reads

$$-i \int d^4x\, e^{-iq\cdot x} \langle p_1' p_2' | T\{J^\mu(x) J^\nu(0)\} | p_1 p_2\rangle = -(2\pi) k_\eta 16\pi B_{\rm diff}\, \phi_{I\!P/N}(x_{I\!P}) \phi_{I\!P/N}(x_{I\!P} - 2\xi_N) \times \frac{1}{x_{I\!P}} H_{I\!P}^{\mu\nu}(\xi_{I\!P}, t, Q^2), \tag{47}$$

where $k_\eta = (1 - i\eta)^2/(1+\eta^2)$, $\eta \approx \pi/2(\alpha_{I\!P}(0) - 1) \approx 0.17$ is the ratio of the real to imaginary parts of the $\gamma^* N \to XN$ diffractive amplitude [11–13], $\phi_{I\!P/N}$ is the probability amplitude of emitting a Pomeron off the nucleon, and $H_{I\!P}^{\mu\nu}$ is the DVCS amplitude on the Pomeron. In our analysis, we take $\phi_{I\!P/N}(x_{I\!P}) = \sqrt{f_{I\!P/p}(x_{I\!P})}$, where the Pomeron flux is defined by Eq. (44). The DVCS amplitude on the Pomeron, $H_{I\!P}^{\mu\nu}$, is modeled by using the PDFs of the Pomeron, $f_{j/I\!P}$, which enter Eq. (43). The t dependence of $H_{I\!P}^{\mu\nu}$ is given by the factor $e^{B_{\rm diff} t}$.

The skewedness $\xi_{I\!P}$ is defined with respect to the Pomeron [compare to Eq. (14)],

$$\xi_{I\!P} = \frac{Q^2}{4\,\bar p_{I\!P}\cdot q} = \frac{\xi_A}{\alpha_1 x_{I\!P} - \xi_A}, \tag{48}$$

where $\bar p_{I\!P} = (p_{I\!P} + p'_{I\!P})/2$ with $p_{I\!P}$ and $p'_{I\!P}$ the momenta of the Pomerons emitted by nucleon 1 and nucleon 2, respectively.

A few words are in order about the remaining factors in Eq. (47). The factor of 2π comes from the standard definition of the connection between the Compton scattering amplitude and the structure functions. The factor of 16π is specific for diffraction and has its origin in the optical theorem (see, e.g., Ref. [11]). Note also the overall minus sign, which is a consequence of the fact that the considered matrix element is essentially a product of two scattering amplitudes, which are predominantly imaginary at high energies.

To implement Eq. (47) in Eq. (36), we insert the following identity in Eq. (36):

$$1 = \int d\alpha_2'\, dx_{I\!P}\, \delta(\alpha_2' - \alpha_2 - \alpha_2(x_{I\!P} - 2\xi_N)) \times \delta(\alpha_1' - \alpha_1 + \alpha_1 x_{I\!P})\alpha_1. \tag{49}$$

Inserting Eq. (47) in Eq. (36), we obtain

$$H_A^{(b)\mu\nu} = -\Re e \left\{ \sum_{\rm pairs} \int \frac{d\alpha_1' d\alpha_2'}{\sqrt{\alpha_1'\alpha_2'}} \frac{d^2\vec k'_{\perp 1}}{16\pi^3} \frac{d\alpha_1 d\alpha_2}{\sqrt{\alpha_1\alpha_2}} \frac{d^2\vec k_{\perp 1} d^2\vec k_{\perp 2}}{(16\pi^3)^2} \times \int_{x_{I\!P}^{\rm min}}^{0.1} dx_{I\!P}\, \delta(\alpha_2' - \alpha_2 - \alpha_2(x_{I\!P} - 2\xi_N)) \times \delta(\alpha_1' - \alpha_1 + \alpha_1 x_{I\!P})\alpha_1 \phi_N^*(\alpha_1', \vec k'_{\perp 1}) \phi_N(\alpha_1, \vec k_{\perp 1}) \times \phi_N^*(\alpha_2', \vec k'_{\perp 2}) \phi_N(\alpha_2, \vec k_{\perp 2}) k_\eta (32\pi^2) \times B_{\rm diff} \phi_{I\!P/N}(x_{I\!P}) \phi_{I\!P/N}(x_{I\!P} - 2\xi_N) \right\} \times \frac{1}{x_{I\!P}} H_{I\!P}^{\mu\nu}(\xi_{I\!P}, t, Q^2), \tag{50}$$

where $x_{I\!P}^{\min} = \max\{x_N, 2\xi_N\}$. The limits of integration over $x_{I\!P}$ deserve a comment. The lower limit of integration is the simultaneous requirement that the Pomeron LC fraction in Eq. (46) is non-negative [see also Fig. 4(b)] and that the Pomeron LC fraction is larger than the LC fraction of the active quark, $x_{I\!P} \geqslant x_N$. The upper limit of integration is the standard condition on the produced diffractive masses, which can be cast in the form $x_{I\!P} \leqslant 0.1$.

In addition, in Eq. (50) we made an assumption that multiple interactions with the target nucleons lead only to the attenuation of $H_A^{(b)\mu\nu}$ and do not introduce an additional imaginary contribution. This amounts to taking the real part of the expression describing the interaction with two nucleons of the target.

For comparison with the predictions of the leading twist theory of nuclear shadowing for nuclear PDFs and for the convenience of numerical calculations, we evaluate the overlap of the nuclear LC wave functions in Eq. (50) in coordinate space. The Fourier transform of the nuclear LC wave function reads

$$\phi_N(\alpha, \vec{k}_\perp) = \sqrt{2m_N} \int dz\, d^2\vec{b} e^{im_N\alpha z + i\vec{k}_\perp\cdot\vec{b}} \phi_N(z, \vec{b}). \quad (51)$$

The normalization of the LC wave function in momentum space [Eq. (25)] fixes the normalization of the wave function in coordinate space,

$$\int dz\, d^2\vec{b} |\phi_N(z, \vec{b})|^2 \equiv \int dz\, d^2\vec{b} \rho_A(z, \vec{b}) = 1, \quad (52)$$

where $\rho_A(z, \vec{b})$ is the nuclear density. We have used that $\alpha \approx 1/A$. In our numerical analysis, we used a two-parameter Fermi form for $\rho_A(z, \vec{b})$ [36].

Thus, substituting Eq. (51) into Eq. (50), using the approximation

$$\frac{\alpha_1}{\sqrt{\alpha_1'\alpha_2'\alpha_1\alpha_2}} \approx A \approx \frac{\xi_N}{\xi_A}, \quad (53)$$

and integrating over the LC fractions and the transverse momenta, we obtain our final expression for $H_A^{(b)\mu\nu}$:

$$\begin{aligned} H_A^{(b)\mu\nu} = &-\frac{A(A-1)}{2}\frac{\xi_N}{\xi_A} 16\pi B_{\rm diff} \Re e \\ &\times \left\{ \int d^2\vec{b} e^{i\vec{\Delta}_\perp\cdot\vec{b}} \int_\infty^\infty dz_1 \int_{z_1}^\infty dz_2 \right. \\ &\times \int_{x_{I\!P}^{\min}}^{0.1} dx_{I\!P}\, \rho_A(b, z_1)\rho_A(b, z_2) \\ &\times k_\eta e^{-im_N z_2(x_{I\!P}-2\xi_N)+im_N z_1 x_{I\!P}} \\ &\left. \times \phi_{I\!P/N}(x_{I\!P})\phi_{I\!P/N}(x_{I\!P}-2\xi_N) \right\} \\ &\times \frac{1}{x_{I\!P}} H_{I\!P}^{\mu\nu}(\xi_{I\!P}, t_{\min}, Q^2), \end{aligned} \quad (54)$$

where we have used $\sum_{\rm pairs} = A(A-1)/2$. Note that to perform the Fourier transform, we neglected the weak t dependence of $H_{I\!P}^{\mu\nu}$ compared to the rapid t dependence of the nuclear distribution and, hence, evaluated $H_{I\!P}^{\mu\nu}$ at the minimal momentum transfer $t_{\min} \approx -m_N^2 x_B^2 \approx 0$. We also introduced the $z_2 > z_1$ ordering to reflect the space-time evolution of $\gamma^* NN \to \gamma NN$ scattering (see also, e.g., Ref. [37]).

Equation (54) can be turned into the relation between the nuclear GPD and GPD of the Pomeron, quite similarly to the corresponding derivation in the previous section. The DVCS amplitude on the Pomeron, $H_{I\!P}^{\mu\nu}$, is expressed in terms of the CFF of the Pomeron, $\mathcal{H}_{I\!P}$, as

$$H_{I\!P}^{\mu\nu}(\xi_{I\!P}, t, Q^2) \approx -g_\perp^{\mu\nu} \mathcal{H}_{I\!P}(\xi_{I\!P}, t, Q^2), \quad (55)$$

where we neglected the same terms as in Eq. (17). Therefore, for the contribution from the graph in Fig. 2(b) to the nuclear CFF we obtain

$$\begin{aligned} \mathcal{H}_A^{(b)} = &-\frac{A(A-1)}{2}\frac{\xi_N}{\xi_A} 16\pi B_{\rm diff} \Re e \left\{ \int d^2\vec{b} e^{i\vec{\Delta}_\perp\cdot\vec{b}} \int_\infty^\infty dz_1 \right. \\ &\times \int_{z_1}^\infty dz_2 \int_{x_{I\!P}^{\min}}^{0.1} dx_{I\!P}\, \rho_A(b, z_1)\rho_A(b, z_2) \\ &\times k_\eta e^{-im_N z_2(x_{I\!P}-2\xi_N)+im_N z_1 x_{I\!P}} \phi_{I\!P/N}(x_{I\!P}) \\ &\left. \times \phi_{I\!P/N}(x_{I\!P}-2\xi_N) \right\} \frac{1}{x_{I\!P}} \mathcal{H}_{I\!P}(\xi_{I\!P}, t_{\min}, Q^2). \end{aligned} \quad (56)$$

To the leading twist accuracy and to the leading order in the strong coupling constant, $\mathcal{H}_{I\!P}$ can be expressed in terms of the GPD of the Pomeron, $H_{I\!P}$, as

$$\begin{aligned} \mathcal{H}_{I\!P}(\xi_{I\!P}, t) = &\int_{-1}^1 dx' H_{I\!P}(x', \xi_{I\!P}, t) \\ &\times \left(\frac{1}{x' - \xi_{I\!P} + i\epsilon} + \frac{1}{x' + \xi_{I\!P} - i\epsilon} \right). \end{aligned} \quad (57)$$

Using the same argument that led to Eq. (30), we find that

$$\frac{x'}{\xi_{I\!P}} = \frac{x}{\xi_A} = \frac{x_N}{\xi_N}, \quad (58)$$

where x parametrizes the interacting quark LC fractions in the graph in Fig. 3(a). Those fractions are equal to $x + \xi_A = (\xi_A/\xi_{I\!P})(x' + \xi_{I\!P})$ and $x - \xi_A = (\xi_A/\xi_{I\!P})(x' - \xi_{I\!P})$, respectively. Since $|x'| \leqslant 1$, we find that $|x| \leqslant \xi_A/\xi_{I\!P}$. Thus, substituting Eq. (56) into the first line of Eq. (28), changing the integration variable from x to x' according to Eq. (58), recalling Eq. (57), and noticing that the ensuing relation holds not only for the DVCS amplitude written to the leading order in the strong coupling constant but also for individual parton flavors, we obtain the contribution of the graph in Fig. 2(b) to the nuclear GPD of flavor j, $H_A^{j(b)}$, as

$$\begin{aligned} &H_A^{j(b)}(x, \xi_A, t, Q^2) \\ &= -\frac{A(A-1)}{2}\frac{\xi_N}{\xi_A} 16\pi B_{\rm diff} \Re e \left\{ \int d^2\vec{b} e^{i\vec{\Delta}_\perp\cdot\vec{b}} \int_\infty^\infty dz_1 \right. \\ &\times \int_{z_1}^\infty dz_2 \int_{x_{I\!P}^{\min}}^{0.1} dx_{I\!P}\, \rho_A(b, z_1)\rho_A(b, z_2) k_\eta \\ &\left. \times e^{-im_N z_2(x_{I\!P}-2\xi_N)+im_N z_1 x_{I\!P}} \phi_{I\!P/N}(x_{I\!P})\phi_{I\!P/N}(x_{I\!P}-2\xi_N) \right\} \\ &\times \frac{1}{x_{I\!P}} H_{I\!P}^j \left(\frac{\xi_{I\!P}}{\xi_N} x_N, \xi_{I\!P}, t_{\min}, Q^2 \right). \end{aligned} \quad (59)$$

The GPD of the Pomeron, $H^j_{I\!P}$, is modeled by using the PDFs of the Pomeron, $f_{j/I\!P}$. In our numerical analysis, we used the model of GPDs in which it is assumed that the effect of skewedness in GPDs can be neglected at the initial evolution scale. This model corresponds to the double distribution model [38] with a δ-function-like profile [39]. The details are given in Sec. IV

C. Quasi-eikonal approximation for multiple rescatterings and the final expression for nuclear PDFs

To evaluate the contribution of the graph in Fig. 2(c), we use the following high-energy (small x_B) space-time development of the process. The virtual photon diffractively interacts with nucleon 1 and produces a certain diffractive state X characterized by $x_{I\!P}$ (diffractive mass M_X). The produced state is then assumed to elastically scatter on $A-2$ nucleons of the target. Finally, the last interaction of the state X with nucleon 2 produces the final real photon. This picture of multiple rescattering at high energy corresponds to the quasi-eikonal approximation for the graph in Fig. 2(c) and higher rescattering terms. The quasi-eikonal approximation was used in the evaluation of nuclear PDFs in the framework of the leading twist theory of nuclear shadowing [11–13] and in the evaluation of the DVCS amplitude on nuclei in the framework of Generalized vector meson dominance model [27].

Within the quasi-eikonal approximation, the multiple interactions can be summed and can be cast in the form of the eikonal attenuation factor,

$$T = e^{-\frac{A}{2}(1-i\eta)\sigma^j_{\rm eff}(x_B,Q^2)\int_{z_1}^{z_2} dz' \rho_A(\vec{b},z')}, \tag{60}$$

where $\sigma^j_{\rm eff}$ is the effective cross section, which determines the strength of the rescattering of the state X off the nucleons. This cross section is defined as [11–13]

$$\sigma^j_{\rm eff}(x_B,Q^2) = \frac{16\pi B_{\rm diff}}{(1+\eta^2)x_B f_{j/N}(x_B,Q^2)} \times \int_{x_B}^{0.1} dx_{I\!P}\, \beta f_{I\!P/p}(x_{I\!P}) f_{j/I\!P}(\beta,Q^2), \tag{61}$$

where $f_{j/N}$ is the usual parton PDF of the nucleon. For a given flavor j, $\sigma^j_{\rm eff}$ is proportional to the probability of diffraction relative to the total probability of the interaction. As an example, we present $\sigma^j_{\rm eff}$ as a function of x_B at fixed $Q^2 = 2.5$ GeV^2 for the $\bar{u}$ quark and gluon flavors in Fig. 6.

Thus, collecting all contributions to the nuclear GPD H^j_A,

$$H^j_A(x,\xi_A,t,Q^2) = H^{j(a)}_A + H^{j(b)}_A + H^{j(c)}_A + \cdots, \tag{62}$$

we obtain our final expression for flavor j GPD of a heavy spinless nucleus:

$$\begin{aligned} &H^j_A(x,\xi_A,t,Q^2) \\ &= \frac{\xi_N}{\xi_A} F_A(t) \sum_N H^j_N(x_N,\xi_N,t,Q^2) \\ &\quad - \frac{A(A-1)}{2}\frac{\xi_N}{\xi_A} 16\pi B_{\rm diff}\, \Re e \Bigg\{ \int d^2\vec{b} e^{i\vec{\Delta}_\perp\cdot\vec{b}} \int_\infty^\infty dz_1 \end{aligned}$$

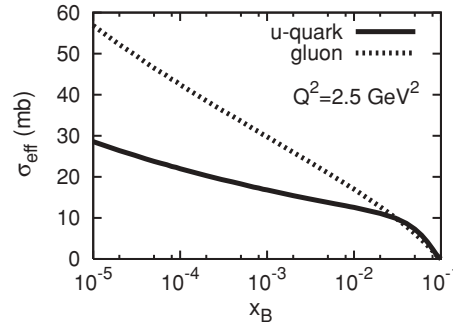

FIG. 6. The effective cross section $\sigma^j_{\rm eff}$ [see Eq. (61)] for the $\bar{u}$ quarks and gluons as a function of Bjorken x_B and at fixed $Q^2 = 2.5$ GeV^2.

$$\begin{aligned} &\times \int_{z_1}^\infty dz_2 \int_{x_{I\!P}^{\rm min}}^{0.1} dx_{I\!P}\, \rho_A(b,z_1)\rho_A(b,z_2) k_\eta \\ &\times e^{-im_N z_2(x_{I\!P}-2\xi_N)+im_N z_1 x_{I\!P}} e^{-\frac{A}{2}(1-i\eta)\sigma^j_{\rm eff}(x_B,Q^2)\int_{z_1}^{z_2} dz' \rho_A(\vec{b},z')} \\ &\times \phi_{I\!P/N}(x_{I\!P})\phi_{I\!P/N}(x_{I\!P}-2\xi_N)\Bigg\} \\ &\times \frac{1}{x_{I\!P}} H^j_{I\!P}\left(\frac{\xi_{I\!P}}{\xi_N}x_N, \xi_{I\!P}, t_{\rm min}, Q^2\right). \end{aligned} \tag{63}$$

For practical applications and for a comparison to the case of a free nucleon, it is convenient to simultaneously rescale the LC fraction x and the nuclear GPDs on the left-hand side of Eq. (63):

$$H^j_A(x,\xi_A,t,Q^2) \to \frac{\xi_N}{\xi_A} H^j_A(x_N,\xi_A,t,Q^2). \tag{64}$$

(where the rescaling of the nuclear GPD is necessary to preserve sum rules involving the nuclear GPD). Then, our master equation for the nuclear GPD becomes

$$\begin{aligned} &H^j_A(x_N,\xi_A,t,Q^2) \\ &= F_A(t) \sum_N H^j_N(x_N,\xi_N,t,Q^2) \\ &\quad - \frac{A(A-1)}{2} 16\pi B_{\rm diff}\, \Re e \Bigg\{ \int d^2\vec{b} e^{i\vec{\Delta}_\perp\cdot\vec{b}} \int_\infty^\infty dz_1 \\ &\quad \times \int_{z_1}^\infty dz_2 \int_{x_{I\!P}^{\rm min}}^{0.1} dx_{I\!P}\, \rho_A(b,z_1)\rho_A(b,z_2) k_\eta \\ &\quad \times e^{-im_N z_2(x_{I\!P}-2\xi_N)+im_N z_1 x_{I\!P}} e^{-\frac{A}{2}(1-i\eta)\sigma^j_{\rm eff}(x_B,Q^2)\int_{z_1}^{z_2} dz' \rho_A(\vec{b},z')} \\ &\quad \times \phi_{I\!P/N}(x_{I\!P})\phi_{I\!P/N}(x_{I\!P}-2\xi_N)\Bigg\} \\ &\quad \times \frac{1}{x_{I\!P}} H^j_{I\!P}\left(\frac{\xi_{I\!P}}{\xi_N}x_N, \xi_{I\!P}, t_{\rm min}, Q^2\right). \end{aligned} \tag{65}$$

As we explained earlier, we neglected the Fermi motion effect in the first term in Eq. (65). If necessary, the Fermi motion effect can be restored by replacing the first term in Eq. (65) by the right-hand side of Eq. (34).

III. NUCLEAR GPDS IN THE $\xi_A \to 0$ LIMIT AND THE SPACIAL IMAGE OF NUCLEAR SHADOWING

In the forward limit, nuclear GPDs reduce to nuclear PDFs,

$$H_A^j(x,0,0,Q^2) = f_{j/A}(x,Q^2). \tag{66}$$

Taking the $\xi_A = t = 0$ limit in Eq. (65), we obtain

$$\begin{aligned} &H_A^j(x_B,0,0,Q^2) \\ &= \sum_N f_{j/N}(x_B,Q^2) - \frac{A(A-1)}{2} 16\pi B_{\rm diff}\,\Re e \\ &\quad\times\left\{\int d^2\vec{b}\int_\infty^\infty dz_1\int_{z_1}^\infty dz_2\int_{x_B}^{0.1} dx_{I\!P} \right. \\ &\quad\times \rho_A(b,z_1)\rho_A(b,z_2)k_\eta \\ &\quad\times e^{im_N x_{I\!P}(z_1-z_2)} e^{-\frac{A}{2}(1-i\eta)\sigma_{\rm eff}^j(x_B,Q^2)\int_{z_1}^{z_2} dz'\rho_A(\vec{b},z')} \\ &\quad\left.\times f_{I\!P/p}(x_{I\!P})\frac{1}{x_{I\!P}} f_{j/I\!P}\left(\beta=\frac{x_B}{x_{I\!P}},Q^2\right)\right\}. \end{aligned} \tag{67}$$

Here we used the fact that, in the $\xi_A \to 0$ limit, $\xi_N, \xi_{I\!P}, t_{\rm min} \to 0$ and $\xi_{I\!P} x_N/\xi_N = x' \to \beta = x_B/x_{I\!P}$. The obtained expression for the nuclear PDF $f_{j/A}$ as a forward limit of the nuclear GPD coincides with the direct calculation of $f_{j/A}$ in the framework of the leading twist theory of nuclear shadowing [11–13]; that is, our master equation [Eq. (65)] has the correct (consistent) forward limit.

Next let us consider the $\xi_A \to 0$ limit (i.e., the limit when the momentum transfer t is purely transverse, $t = -\Delta_\perp^2$). Taking the $\xi_A \to 0$ limit in Eq. (65), we obtain

$$\begin{aligned} &H_A^j(x_N,0,t,Q^2) \\ &= F_A(t)\sum_N H_N^j(x_N,0,t,Q^2) - \frac{A(A-1)}{2} \\ &\quad\times 16\pi B_{\rm diff}\Re e\left\{\int d^2\vec{b} e^{i\vec{\Delta}_\perp\cdot\vec{b}}\int_\infty^\infty dz_1\int_{z_1}^\infty dz_2\int_{x_N}^{0.1} dx_{I\!P}\right. \\ &\quad\times \rho_A(b,z_1)\rho_A(b,z_2)k_\eta \\ &\quad\times e^{im_N x_{I\!P}(z_1-z_2)} e^{-\frac{A}{2}(1-i\eta)\sigma_{\rm eff}^j(x_B,Q^2)\int_{z_1}^{z_2} dz'\rho_A(\vec{b},z')} \\ &\quad\left.\times f_{I\!P/p}(x_{I\!P})\frac{1}{x_{I\!P}} f_{j/I\!P}\left(\frac{x_N}{x_{I\!P}},Q^2\right)\right\}. \end{aligned} \tag{68}$$

Again, we used the fact that, in the $\xi_A \to 0$ limit, $\xi_N, \xi_{I\!P}, t_{\rm min} \to 0$, $\xi_{I\!P} x_N/\xi_N \to x_N/x_{I\!P}$, and $H_{I\!P}^j(\frac{\xi_{I\!P}}{\xi_N}x_N, \xi_{I\!P}, t_{\rm min}, Q^2) \to f_{j/I\!P}(x_N/x_{I\!P}, Q^2)$. Note also the lower limit of integration over $x_{I\!P}$, $x_{I\!P}^{\rm min} = x_N$. Since the t dependence of the nuclear form factor, $F_A(t)$, is much faster than that of the nucleon GPD $H_N^j(x_N,0,t,Q^2)$, the latter can be evaluated at $t=0$ (i.e., in the forward limit). Then, Eq. (68) becomes

$$\begin{aligned} &H_A^j(x_N,0,t,Q^2) \\ &= F_A(t)\sum_N f_{j/N}(x_N,Q^2) \\ &\quad - \frac{A(A-1)}{2} 16\pi B_{\rm diff}\Re e\left\{\int d^2\vec{b} e^{i\vec{\Delta}_\perp\cdot\vec{b}}\int_\infty^\infty dz_1\int_{z_1}^\infty dz_2\right. \\ &\quad\times\int_{x_N}^{0.1} dx_{I\!P}\,\rho_A(b,z_1)\rho_A(b,z_2)k_\eta \\ &\quad\times e^{im_N x_{I\!P}(z_1-z_2)} e^{-\frac{A}{2}(1-i\eta)\sigma_{\rm eff}^j(x_B,Q^2)\int_{z_1}^{z_2} dz'\rho_A(\vec{b},z')} \\ &\quad\left.\times f_{I\!P/p}(x_{I\!P})\frac{1}{x_{I\!P}} f_{j/I\!P}\left(\frac{x_N}{x_{I\!P}},Q^2\right)\right\}. \end{aligned} \tag{69}$$

In the case of nucleon GPDs, the interpretation of GPDs in the $\xi \to 0$ limit is given in the impact parameter representation, where the GPDs have the meaning of the probability densities [7]. We shall also analyze our nuclear GPDs in the $\xi_A \to 0$ limit in the impact parameter space. To this end, we introduce the nuclear GPD in the impact parameter space,

$$\begin{aligned} &H_A^j(x,0,\vec{b},Q^2) \\ &= \int\frac{d^2\vec{\Delta}_\perp}{(2\pi)^2} e^{-i\vec{\Delta}_\perp\cdot\vec{b}} H_A^j(x,0,t=-\Delta_\perp^2,Q^2). \end{aligned} \tag{70}$$

The Fourier transform of Eq. (69) gives

$$\begin{aligned} &H_A^j(x_N,0,\vec{b},Q^2) \\ &= T_A(b)\sum_N f_{j/N}(x_N,Q^2) - \frac{A(A-1)}{2} \\ &\quad\times 16\pi B_{\rm diff}\Re e\left\{\int_\infty^\infty dz_1\int_{z_1}^\infty dz_2\int_{x_N}^{0.1} dx_{I\!P}\right. \\ &\quad\times \rho_A(b,z_1)\rho_A(b,z_2) e^{im_N x_{I\!P}(z_1-z_2)} \\ &\quad\times e^{-\frac{A}{2}(1-i\eta)\sigma_{\rm eff}^j(x_B,Q^2)\int_{z_1}^{z_2} dz'\rho_A(\vec{b},z')} \\ &\quad\left.\times f_{I\!P/p}(x_{I\!P})\frac{1}{x_{I\!P}} f_{j/I\!P}\left(\frac{x_N}{x_{I\!P}},Q^2\right)\right\}, \end{aligned} \tag{71}$$

where $T_A(b) = \int dz \rho_A(b,z)$ and $\rho_A(b,z)$ is the nuclear density [see Eq. (52)]. It is important to note that the nuclear GPD $H_A^j(x_N,0,\vec{b},Q^2)$ given by Eq. (71) is nothing else but the impact-parameter-dependent nuclear PDF introduced and discussed in the framework of the leading twist nuclear shadowing [11–13].

In Eq. (71), the first term is the Born approximation to H_A^j corresponding to the graph in Fig. 2(a); the second term is the nuclear shadowing correction corresponding to the graphs in Figs. 2(b) and 2(c) and to higher rescattering terms not shown in Fig. 2. We quantify the magnitude of the nuclear shadowing correction by considering the ratio

$$R^j(x_N,b,Q^2) = \frac{H_A^j(x_N,0,\vec{b},Q^2)}{T_A(b)\sum_N f_{j/N}(x_N,Q^2)}, \tag{72}$$

where the numerator is given by Eq. (71). In the absence of nuclear shadowing, $R^j(x_N,b,Q^2) = 1$. The ratio $R^j(x_N,b,Q^2)$ for the nucleus of ^{208}Pb as a function of x_N and b at fixed $Q^2 = 2.5$ GeV^2 is presented in Fig. 7. In the figure, the top panel corresponds to $\bar{u}$ quarks; the bottom panel corresponds to gluons.

Essentially, Fig. 7 presents the impact parameter dependence of nuclear shadowing, or the spacial image of nuclear shadowing. Several features of Fig. 7 deserve mentioning. First, the amount of nuclear shadowing [the deviation of $R^j(x_N,b,Q^2)$ from unity] increases as one decreases x_N and b. Second, nuclear shadowing for gluons is larger than

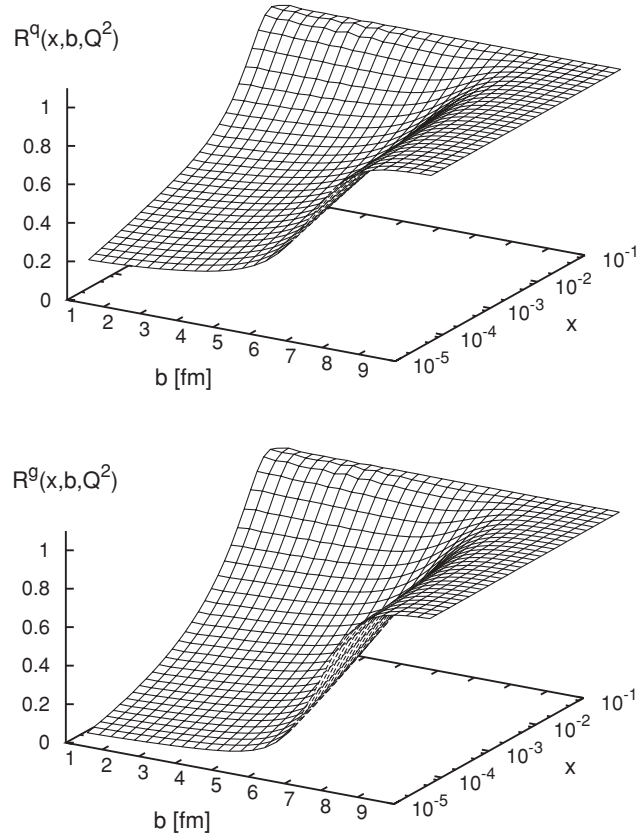

FIG. 7. Impact parameter dependence of nuclear shadowing for ^{208}Pb. The graphs show the ratio $R^j(x_N, b, Q^2)$ of Eq. (72) as a function of the LC fraction x_N and the impact parameter b at fixed $Q^2 = 2.5$ GeV^2. The top panel corresponds to $\bar{u}$ quarks; the bottom panel corresponds to gluons.

for quarks. For instance, at $x_N = 10^{-5}$ and at $b = 0$, $R^g = 0.073$, but $R^q = 0.23$. Third, nuclear shadowing induces nontrivial correlations between x_N and b in the nuclear GPD $H_A^j(x, 0, \vec{b}, Q^2)$, even if such correlations are absent in the free nucleon GPD. [In Eq. (71) we neglected the x_N-b correlations in the nucleon GPDs by neglecting the t dependence of $H_N^j(x_N, 0, t, Q^2)$.] In this respect, the spacial image of nuclear GPDs at small x_N is very different from the case of the free nucleon: Whereas the free nucleon GPDs become independent of b in the $x_N \to 0$ limit [7], the suppression of nuclear GPDs by nuclear shadowing is strongly correlated with the impact parameter b.

IV. NUCLEAR SHADOWING AND PREDICTIONS FOR NUCLEAR DVCS OBSERVABLES

It is convenient to quantify the amount of nuclear shadowing in our master expression for the nuclear GPD of a heavy nucleus [Eq. (65)] in terms of the $R^j(x_N, \xi_N, t, Q^2)$ ratio, which we define as

$$R^j(x_N, \xi_N, t, Q^2) \equiv \frac{H_A^j(x_N, \xi_A, t, Q^2)}{F_A(t) \sum_N H_N^j(x_N, \xi_N, t, Q^2)}$$

$$= 1 - \frac{A(A-1)}{2} 16\pi B_{\rm diff} \Re e \left\{ \int d^2\vec{b} e^{i\vec{\Delta}_\perp \cdot \vec{b}} \int_\infty^\infty dz_1 \right.$$

$$\times \int_{z_1}^\infty dz_2 \int_{x_{I\!P}^{\min}}^{0.1} dx_{I\!P} \times \rho_A(b, z_1)\rho_A(b, z_2) k_\eta$$

$$\times e^{-im_N z_2 (x_{I\!P} - 2\xi_N) + im_N z_1 x_{I\!P}} e^{-\frac{A}{2}(1-i\eta)\sigma_{\rm eff}^j(x_B, Q^2)\int_{z_1}^{z_2} dz' \rho_A(\vec{b}, z')}$$

$$\left. \times \phi_{I\!P/N}(x_{I\!P}) \phi_{I\!P/N}(x_{I\!P} - 2\xi_N) \right\}$$

$$\times \frac{1}{x_{I\!P}} H_{I\!P}^j \left(\frac{\xi_{I\!P}}{\xi_N} x_N, \xi_{I\!P}, t_{\min}, Q^2 \right) \Big/$$

$$\times \left(F_A(t) \sum_N H_N^j(x_N, \xi_N, t, Q^2) \right). \quad (73)$$

In the absence of nuclear shadowing (and the Fermi motion effect), $R^j(x_N, \xi_N, t, Q^2) = 1$. The ratio $R^j(x_N, \xi_N, t, Q^2)$ is a generalization and a Fourier transform of the ratio $R^j(x_N, b, Q^2)$ of Eq. (72).

At high energies, scattering amplitudes are predominantly imaginary. As follows from Eq. (28), to the leading twist accuracy and to the leading order in α_s, the imaginary part of the DVCS amplitude (the CFF) reads

$$\Im m \mathcal{H}_A(\xi_A, t, Q^2) = -\pi H_A(\xi_A, \xi_A, t, Q^2), \quad (74)$$

where

$$H_A(\xi_A, \xi_A, t) = \sum_{q,\bar{q}} e_q^2 H_A^q(\xi_A, \xi_A, t). \quad (75)$$

Therefore, in our numerical analysis that follows, we shall present our predictions for $R^j(\xi_N, \xi_N, t, Q^2)$.

In our numerical analysis, we use the model of GPDs of the free nucleon and the Pomeron, in which it is assumed that the effect of skewedness in GPDs can be neglected at the initial QCD evolution scale ($Q_0^2 = 2.5$ GeV^2 in our case). Then, in the $x_N = \xi_N$ case of interest, one has

$$H_N^j(\xi_N, \xi_N, Q_0^2) = f_{j/N}(\xi_N, Q_0^2),$$
$$H_{I\!P}^j(\xi_{I\!P}, \xi_{I\!P}, Q_0^2) = f_{j/I\!P}(\xi_{I\!P}, Q_0^2) = f_{j/I\!P}\left(\frac{\xi_N}{x_{I\!P}}, Q_0^2 \right). \quad (76)$$

This model corresponds to the double distribution parametrization of GPDs [38] with a δ-function-like profile [39]; we shall refer to this model of the GPDs as the forward-like model. Note that the suggestion that the GPDs at small x_B and at the low input scale Q_0^2 can be well approximated by the usual forward PDFs was first proposed in Ref. [40].

It is very important to point out that the recent analysis of the high-energy HERA data on DVCS on the proton unambiguously indicated that the description of the data at leading order accuracy requires almost no skewedness effect in the input GPDs [41]. This clearly favors the forward-like model of the PDFs over other small-x_B parametrizations (see, e.g., Ref. [42]).

Let us first examine the $R^j(\xi_N, \xi_N, t, Q^2)$ ratio of Eq. (73) in the situation when the momentum transfer t is purely longitudinal, $\vec{\Delta}_\perp = 0$ and $t = t_{\min} \approx -4\xi_N^2 m_N^2$. Figure 8 presents $R^j(\xi_N, \xi_N, t, Q^2)$ for ^{208}Pb as a function of Bjorken x_B at fixed $Q_0^2 = 2.5$ GeV^2 (solid curves). Also, for comparison with nuclear shadowing in usual nuclear PDFs, we present the

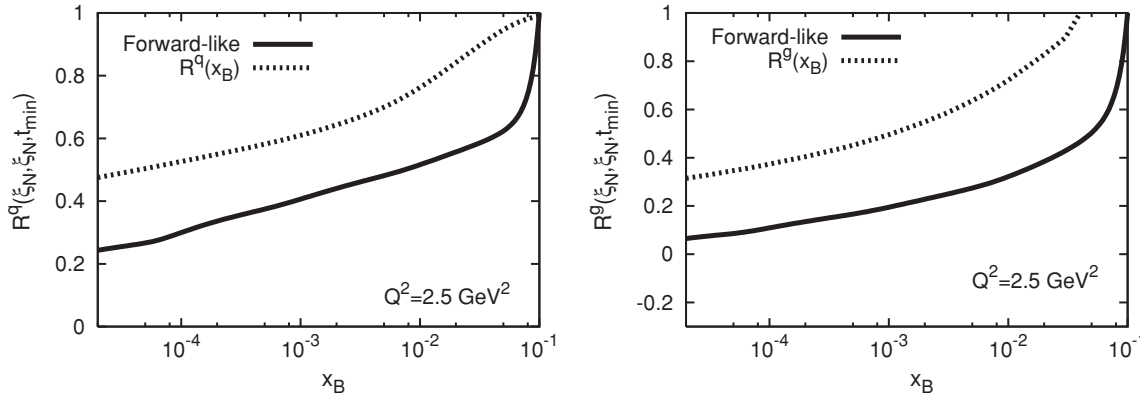

FIG. 8. Nuclear shadowing for the DVCS amplitude for ^{208}Pb at $\vec{\Delta}_\perp = 0$. The plots show the ratio $R^j(\xi_N, \xi_N, t, Q^2)$ of Eq. (73) as a function of x_B at fixed $Q_0^2 = 2.5$ GeV^2 for the forward-like model of GPDs (solid curves). For comparison, the ratio of the usual nuclear to nucleon PDFs, $R^j(x_B) = f_{j/A}(x_B, Q_0^2)/[A f_{j/N}(x_B, Q_0^2)]$, is given by the dotted curves. The left panel corresponds to $\bar{u}$ quarks; the right panel corresponds to gluons.

ratio $R^j(x_B) = f_{j/A}(x_B, Q_0^2)/[A f_{j/N}(x_B, Q_0^2)]$ by the dotted curves [13]. The left panel corresponds to $\bar{u}$ quarks; the right panel corresponds to gluons.

As one can see from Fig. 8, the suppression of $R^j(\xi_N, \xi_N, t, Q_0^2)$ by nuclear shadowing is very large and it is larger than the suppression of $R^j(x_B, Q_0^2)$ in the forward case. This is one of new results of this work and it comes from our model for the graph in Fig. 4(b). In particular, we assumed that the matrix element

$$\langle p_1' p_2' | T\{J^\mu(x) J^\nu(0)\} | p_1 p_2 \rangle \propto \phi_{I\!P/N}(x_{I\!P}) \phi_{I\!P/N}(x_{I\!P} - 2\xi_N), \tag{77}$$

which leads to the dynamical enhancement of nuclear shadowing because $\phi_{I\!P/N}(x_{I\!P} - 2\xi_N) \gg \phi_{I\!P/N}(x_{I\!P})$ for $x_{I\!P}$ close to $2\xi_N$.

We stress that our results presented in Fig. 8 have an exploratory character and are subject of significant theoretical uncertainties, which include our modeling of the $\langle p_1' p_2' | T\{J^\mu(x) J^\nu(0)\} | p_1 p_2 \rangle$ matrix element, the choice of the model for the nucleon and Pomeron GPDs, and the extrapolation of the fits for diffractive PDFs $f_{I\!P}^j$ to unmeasured kinematic regions.

We also mention that the rapid approach of $R^j(\xi_N, \xi_N, t, Q_0^2)$ to unity as $x_B \to 0.1$ is driven both by the decrease of the nuclear shadowing term and by the decrease of the Born term driven by the nuclear form factor at $t = t_{\min} \approx -x_B^2 m_N^2$, $F_A(t_{\min})$.

Next we examine the ratio $R^j(\xi_N, \xi_N, t, Q^2)$ at fixed t as a function of x_B. In this case, the transverse momentum transfer is no longer vanishing: $|\vec{\Delta}_\perp|^2 \approx -4\xi_N^2 m_N^2 - t$. Our results are presented in Fig. 9. The left panel corresponds to $\bar{u}$ quarks; the right panel corresponds to gluons. The solid curves correspond to $t = -0.005$ GeV^2; the dotted curves correspond to $t = -0.01$ GeV^2. For comparison, the ratio $R^j(\xi_N, \xi_N, t_{\min}, Q^2)$ at $t = t_{\min}$ is given by the dot-dashed curves (the same curves as in Fig. 8).

As one can see from Fig. 9, the effect of nuclear shadowing [the deviation of $R^j(\xi_N, \xi_N, t, Q^2)$ from unity at small x_B] increases with increasing $|t|$. This is a natural consequence of the fact that the Born term, whose t dependence is given by

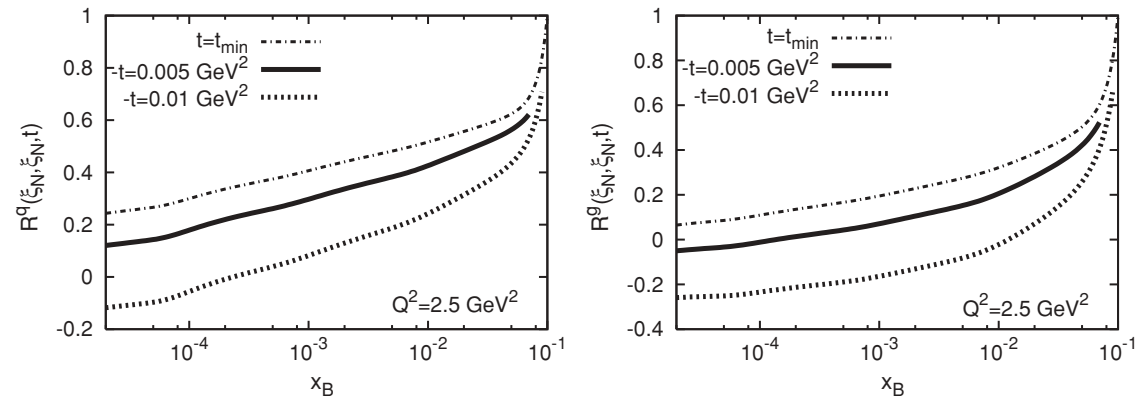

FIG. 9. Nuclear shadowing for the DVCS amplitude for ^{208}Pb at fixed t. The plots show the ratio $R^j(\xi_N, \xi_N, t, Q^2)$ of Eq. (73) as a function of x_B at fixed $Q_0^2 = 2.5$ GeV^2. The left panel corresponds to $\bar{u}$ quarks; the right panel corresponds to gluons. The solid curves correspond to $t = -0.005$ GeV^2; the dotted curves correspond to $t = -0.01$ GeV^2. For comparison, the ratio $R^j(\xi_N, \xi_N, t_{\min}, Q^2)$ at $t = t_{\min}$ is given by the dot-dashed curves.

$F_A(t)$, decreases with increasing $|t|$ faster than the shadowing correction term.

Next we turn to a discussion of the observables measured in DVCS. In lepton-nucleus scattering, it is convenient and natural to use the invariant energy per nucleon. For our results presented in the following, this means that we replace $\xi_A \to \xi_N$ and assume that the invariant energy, $\sqrt{s}$, is given per nucleon. Results of high-energy DVCS measurements are usually presented in terms of the DVCS cross section at the photon level,

$$\frac{d\sigma_{\rm DVCS}}{dt} = \frac{\pi\alpha_{\rm em}^2 x_B^2}{Q^4}|\mathcal{A}_{\rm DVCS}(\xi_N, t, Q^2)|^2, \tag{78}$$

where $\alpha_{\rm em}$ is the fine-structure constant. For the DVCS amplitude at high energies, we use the leading twist and leading order in α_s expression [see Eqs. (74) and (75)],

$$|\mathcal{A}_{\rm DVCS}(\xi_N, t, Q^2)|^2 \approx |\mathcal{H}_A(\xi_N, t, Q^2)|^2 \approx \pi^2[H_A(\xi_N, \xi_N, t, Q^2)]^2, \tag{79}$$

where $H_A(\xi_N, \xi_N, t) = \sum_{q,\bar q} e_q^2 H_A^q(\xi_N, \xi_N, t)$ and $H_A^q(\xi_N, \xi_N, t)$ are given by our master equation [Eq. (65)]. Since gluons enter the DVCS amplitude at the one-loop level, we do not use our results for the gluon nuclear GPD in our calculations presented in the following. Note also that since we do our calculations at fixed $Q_0^2 = 2.5$ GeV^2, we use four quark flavors.

The DVCS process competes with the purely electromagnetic BH process. The BH cross section at the photon level can be written in the following form (see, e.g., Ref. [39]):

$$\frac{d\sigma_{\rm BH}}{dt} = \frac{\pi\alpha_{\rm em}^2}{4Q^2 t(1-y+y^2/2)} \times \int_0^{2\pi}\frac{d\phi}{2\pi}\frac{1}{\mathcal{P}_1(\phi)\mathcal{P}_2(\phi)}|\mathcal{A}_{\rm BH}(\xi_N, t, Q^2)|^2, \tag{80}$$

where y is the fractional energy loss of the incoming lepton, ϕ is the angle between the lepton and hadron scattering planes, $\mathcal{P}_1$ and $\mathcal{P}_2$ are proportional to the lepton propagators, and $|\mathcal{A}_{\rm BH}(\xi_N, t, Q^2)|^2$ is the BH amplitude squared, which can be expressed in terms of its Fourier harmonics $c_n^{\rm BH}$ [39] as

$$|\mathcal{A}_{\rm BH}(\xi_N, t, Q^2, \phi)|^2 = c_0^{\rm BH} + \sum_{n=1}^{2} c_n^{\rm BH}\cos(n\phi). \tag{81}$$

The Fourier harmonics for a spinless target are given in Ref. [43]. For the case of a spinless nucleus, $|\mathcal{A}_{\rm BH}(\xi_N, t, Q^2)|^2 \propto [F_A(t)]^2$; see further details in Ref. [44].

Figure 10 presents our predictions for $d\sigma_{\rm DVCS}/dt$ and $d\sigma_{\rm BH}/dt$ for ^{208}Pb as a function of $|t|$ at fixed $Q_0^2 = 2.5$ GeV^2 and $x_B = 0.001$. In addition to the input just discussed, for the evaluation of the BH cross section, we used $y = 0.31$, which corresponds to the highest among discussed energy options of the future Electron-Ion Collider (EIC), $E_{\rm lepton} = 20$ GeV and $E_{\rm nucleus} = 100$ GeV/nucleon [18,19]. Also, for comparison, we give the DVCS cross section on the proton in the same kinematics (dot-dashed curves).

Several features of Fig. 10 deserve a discussion. First, the t dependence of the BH and DVCS cross sections repeats the pattern of $[F_A(t)]^2$ with several distinct minima. In the case of the DVCS cross section, the minima are shifted by the presence of the shadowing correction. Second, at small $|t|$, the BH cross section is much larger than the DVCS cross section owing to the enhancement by the $1/t$ kinematics factor [see Eq. (80)]. As one increases $|t| > |t_{\rm min}|$, the two cross sections become compatible. Moreover, near minima of the nuclear form factor, the BH cross section becomes very small and, hence, the process is dominated by the DVCS cross section. *Therefore, the measurement of the $eA \to e\gamma A$ differential cross section at the momentum transfer t near the minima of the nuclear form factor will provide a clean probe of nuclear shadowing in nuclear GPDs and nuclear DVCS owing to the suppressed BH background and the suppressed unshadowed Born contribution to the DVCS amplitude.*

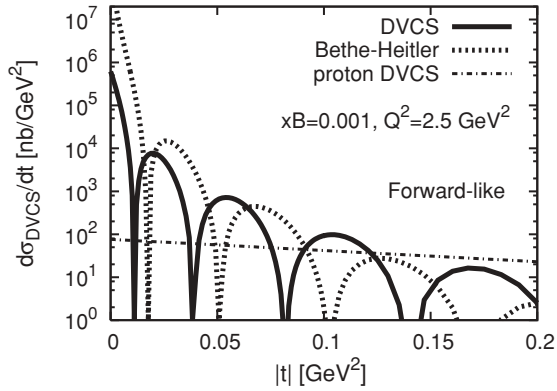

FIG. 10. Nuclear DVCS and BH cross sections for ^{208}Pb as a function of $|t|$ at fixed $Q_0^2 = 2.5$ GeV^2 and $x_B = 0.001$. For comparison, the DVCS cross section on the proton is given by the dot-dashed curves. For the evaluation of the BH cross section, we used $y = 0.31$ (see the text).

Next we study the t-integrated DVCS and BH cross sections at the photon level,

$$\sigma_{\rm DVCS} = \int_{-1\,{\rm GeV}^2}^{t_{\rm min}} dt\,\frac{\sigma_{\rm DVCS}}{dt}, \qquad \sigma_{\rm BH} = \int_{-1\,{\rm GeV}^2}^{t_{\rm min}} dt\,\frac{\sigma_{\rm BH}}{dt}. \tag{82}$$

Figure 11 presents the t-integrated DVCS and BH cross sections for ^{208}Pb as a function of x_B at fixed $Q_0^2 = 2.5$ GeV^2. For comparison, the dot-dashed curve shows the DVCS cross section on the proton in the same kinematics. For the BH cross section, we give two curves, which correspond to two different values of the c.m. lepton-nucleus energy $\sqrt{s}$: The upper curves correspond to the low-energy option for the future EIC, $E_{\rm lepton} = 5$ GeV and $E_{\rm nucleus} = 50$ GeV/nucleon ($\sqrt{s} = 32$ GeV); the lower curves correspond to the high-energy option with $E_{\rm lepton} = 20$ GeV and $E_{\rm nucleus} = 100$ GeV/nucleon ($\sqrt{s} = 90$ GeV) [18,19].

As one see from Fig. 11, in the discussed kinematics, the BH cross section is much larger than the DVCS cross section for $x_B < 0.01$ for both considered high-energy options (lower BH curve) and for $x_B < 0.05$ for the low-energy option (upper BH curve). Therefore, as far as the t-integrated $eA \to e\gamma A$ cross section is concerned, it appears rather challenging to extract a small DVCS signal on the background of the dominant BH

contribution. However, the high luminosity of the future EIC should allow one to measure the t dependence of the DVCS and BH cross sections, which will tremendously increase the potential to probe nuclear GPDs in the domain of nuclear shadowing (small x_B) (see Fig. 10 and the previous discussion).

Another possibility to study nuclear GPDs in the small-x_B region is given by the measurement of DVCS cross section asymmetries (with polarized lepton beams or with lepton beams with the opposite electric charges), which are proportional to the interference between the DVCS and BH amplitudes. As an example, we consider the DVCS beam-spin asymmetry, A_{LU}, measured with the polarized lepton beam and an unpolarized target (which is always the case for spin-0 nuclei that we consider). To the leading twist accuracy, the expression for A_{LU} for a spinless nuclear target reads [39,43,44]

$$A_{LU}(\phi) = -\frac{8K(2-y)ZF_A(t)\Im m\mathcal{H}_A(\xi_N, t, Q^2)\sin\phi}{\frac{1}{x_B}|\mathcal{A}_{\rm BH}(\xi_N, t, Q^2, \phi)|^2 + \frac{x_B\, t\, \mathcal{P}_1(\phi)\mathcal{P}_2(\phi)}{Q^2} 4(1-y+y^2/2)|\Im m\mathcal{H}_A(\xi_N, t, Q^2)|^2}, \tag{83}$$

where $K \propto \sqrt{t_{\rm min} - t}$ is the kinematic factor [39], Z is the nuclear charge, $\Im m\mathcal{H}_A$ is the imaginary part of the nuclear DVCS amplitude given by Eqs. (74), (75), and (65), $|\mathcal{A}_{\rm BH}(\xi_A, t, Q^2, \phi)|^2$ is the square of the BH amplitude [Eq. (81)], and the minus in front corresponds to the electron beam. To consistently work to the leading twist accuracy, one should use only the leading twist contributions to $\mathcal{P}_1(\phi)$, $\mathcal{P}_2(\phi)$, and $|\mathcal{A}_{\rm BH}|^2$ in Eq. (83). However, in the kinematics that we consider, $t < 0.2$ GeV^2, $Q^2 = 2.5$ GeV^2, and $\phi = 90^\circ$, the higher twist corrections are either absent (the terms being proportional to $\cos\phi$) or numerically insignificant, so that we simply use the standard expressions for $\mathcal{P}_1(\phi)$, $\mathcal{P}_2(\phi)$, and $|\mathcal{A}_{\rm BH}|^2$ [39].

Figure 12 presents our predictions for $A_{LU}(\phi)$ as a function of t at fixed $x_B = 0.001$, $Q_0^2 = 2.5$ GeV^2, and the angle $\phi = 90^\circ$. For a comparison, the dotted curve presents A_{LU} for the proton in the same kinematics. Both curves correspond to the incoming lepton fractional energy loss $y = 0.31$, which in turn corresponds to the high-energy option of the future EIC with $E_{\rm lepton} = 20$ GeV and $E_{\rm nucleus} = 100$ GeV/nucleon.

Our predictions for A_{LU} for ^{208}Pb are rather remarkable. The sole reason for the oscillations of A_{LU} for ^{208}Pb is nuclear shadowing! The trend of the oscillations can be understood as follows. At $t = t_{\rm min}$, $A_{LU} = 0$ because of the kinematic factor $K = 0$ (resulting from the vanishing $|\vec{\Delta}_\perp| = 0$). As one slightly increases $|t| > |t_{\rm min}|$, the kinematic factors rapidly increase A_{LU} (which is clearly seen for the proton), but, at the same time, the nuclear shadowing correction decreases the imaginary part of the nuclear DVCS amplitude, $\Im m\mathcal{H}_A$. As a result, A_{LU} increases, but not as rapidly as for the free proton case. At some rather small values of t, $|t| \approx 0.01$ GeV^2 (a value that can be read off the left panel of Fig. 9), $\Im m\mathcal{H}_A$ changes sign and A_{LU} goes through zero. Note that, at this value of t, the nuclear form factor, $F_A(t)$, is still positive. As one increases $|t|$ further, $|\Im m\mathcal{H}_A|$ increases, which increases $|A_{LU}|$ (with both $\Im m\mathcal{H}_A$ and A_{LU} being negative at this point). As $|t|$ is increased even further, the nuclear form factor $F_A(t)$ changes sign and makes A_{LU} positive. The asymmetry stays positive until $\Im m\mathcal{H}_A$ changes sign and becomes positive again [the form factor $F_A(t)$ still being negative]. As $|t|$ is increased, the mechanism of the oscillations just described repeats itself.

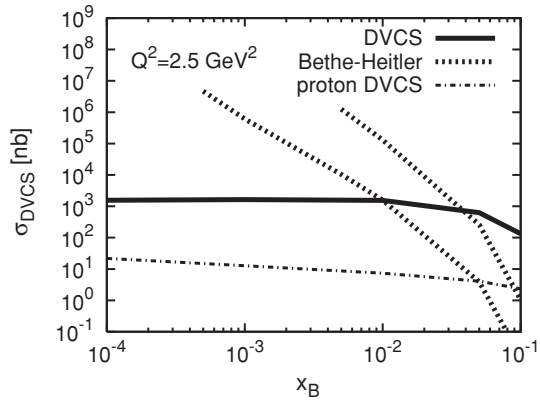

FIG. 11. The t-integrated nuclear DVCS and BH cross sections for ^{208}Pb as a function of x_B at fixed $Q_0^2 = 2.5$ GeV^2. For comparison, the DVCS cross section on the proton is given by the dot-dashed curves. For the evaluation of the BH cross section, we used two energy settings: $\sqrt{s} = 32$ GeV (the upper dashed curve) and $\sqrt{s} = 90$ GeV (the lower dashed curve) (see the text).

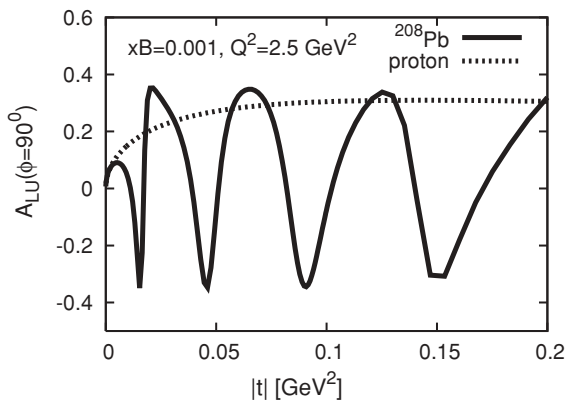

FIG. 12. The DVCS beam-spin asymmetry, $A_{LU}(\phi = 90^\circ)$, for ^{208}Pb as a function of t at fixed $x_B = 0.001$ and $Q_0^2 = 2.5$ GeV^2 (solid curve). For a comparison, the dotted curve presents A_{LU} for the proton in the same kinematics. The calculations correspond to $y = 0.31$.

We emphasize that the oscillations of A_{LU} are caused by nuclear shadowing that has a weaker t dependence than that of the Born contribution [see Eq. (65)]. If the shadowing correction in Eq. (65) is neglected, then the t dependence of the DVCS and BH contributions is the same and is given by the nuclear form factor $F_A(t)$. Then, in the expression for the beam-spin asymmetry, A_{LU}, the t dependence from $F_A(t)$ cancels and A_{LU} for a heavy nuclear target has the same t dependence as A_{LU} for the free proton (i.e., without the oscillations).

V. SUMMARY AND DISCUSSION

We generalized the leading twist theory of nuclear shadowing for usual nuclear parton distributions to nuclear generalized parton distributions for quarks and gluons. We estimated quark and gluon GPDs of spinless nuclei and found very large nuclear shadowing.

In the limit that the momentum transfer is purely transverse, $\xi_A = \xi_N = 0$, after Fourier transform, our nuclear GPDs become impact-parameter-dependent nuclear PDFs. Nuclear shadowing induces nontrivial correlations between the impact parameter b and the light-cone fraction x.

Using our expressions for nuclear GPDs, we made predictions for the cross section of deeply virtual Compton scattering on the heavy nucleus of ^{208}Pb at high energies (in the kinematics of the future EIC). We also calculated the cross section of the purely electromagnetic Bethe-Heitler process and addressed the issue of the extraction of the DVCS signal, and, hence, the extraction of information on nuclear GPDs and nuclear shadowing, from the measurement of the $eA \to e\gamma A$ process. Based on our studies, we can propose two strategies. First, the $eA \to e\gamma A$ differential cross section at the momentum transfer t near the minima of the nuclear form factor is dominated by the DVCS cross section, which should allow for a clear extraction of the latter. Second, nuclear shadowing leads to dramatic oscillations of the DVCS beam-spin asymmetry, A_{LU}, as a function of t. The position of the points where A_{LU} changes sign is directly related to the magnitude of nuclear shadowing.

It is important to note that the t variations of the DVCS and BH differential cross sections and the DVCS beam-spin asymmetry, A_{LU}, are very rapid, with a typical frequency of the order of $1/R_A^2$. This certainly poses a challenge for any future experiments since a rather high resolution in t will be required.

One should also note that nuclear GPDs at small x will be accessed in ultraperipheral nucleus-nucleus collisions at the LHC [45]. In these collisions, the involved nuclei serve as sources of real photons, which enables one to study photon-nuclear interactions at energies up to ten times larger than those achieved at HERA. Nuclear GPDs will be accessed in exclusive photoproduction of heavy vector mesons [46] and lepton pairs [47].

ACKNOWLEDGMENTS

We would like to thank M. Strikman for useful discussions. This paper is authored by Jefferson Science Associates, LLC under US DOE Contract No. DE-AC05-06OR23177. The US Government retains a non-exclusive, paid-up, irrevocable, world-wide license to publish or reproduce this manuscript for US Government purposes.

[1] D. Mueller, D. Robaschik, B. Geyer, F. M. Dittes, and J. Horejsi, Fortschr. Phys. **42**, 101 (1994).
[2] X. D. Ji, J. Phys. G **24**, 1181 (1998).
[3] K. Goeke, M. V. Polyakov, and M. Vanderhaeghen, Prog. Part. Nucl. Phys. **47**, 401 (2001).
[4] M. Diehl, Phys. Rep. **388**, 41 (2003).
[5] A. V. Belitsky and A. V. Radyushkin, Phys. Rep. **418**, 1 (2005).
[6] S. Boffi and B. Pasquini, Riv. Nuovo Cimento **30**, 387 (2007).
[7] M. Burkardt, Int. J. Mod. Phys. A **18**, 173 (2003).
[8] X. D. Ji, Phys. Rev. D **55**, 7114 (1997).
[9] J. C. Collins and A. Freund, Phys. Rev. D **59**, 074009 (1999).
[10] J. C. Collins, L. Frankfurt, and M. Strikman, Phys. Rev. D **56**, 2982 (1997).
[11] L. Frankfurt and M. Strikman, Eur. Phys. J. A **5**, 293 (1999).
[12] L. Frankfurt, V. Guzey, M. McDermott, and M. Strikman, J. High Energy Phys. 02 (2002) 027.
[13] L. Frankfurt, V. Guzey, and M. Strikman, Phys. Rev. D **71**, 054001 (2005).
[14] L. L. Frankfurt and M. I. Strikman, Phys. Rep. **160**, 235 (1988).
[15] M. Arneodo, Phys. Rep. **240**, 301 (1994).
[16] D. F. Geesaman, K. Saito, and A. W. Thomas, Annu. Rev. Nucl. Part. Sci. **45**, 337 (1995).
[17] G. Piller and W. Weise, Phys. Rep. **330**, 1 (2000).
[18] A. Deshpande, R. Milner, R. Venugopalan, and W. Vogelsang, Annu. Rev. Nucl. Part. Sci. **55**, 165 (2005).
[19] C. Aidala *et al.*, White Paper prepared for the NSAC LRP 2007, April 4, 2007, available at http://www.eic.bnl.gov/.
[20] V. N. Gribov, Sov. Phys. JETP **29**, 483 (1969) [Zh. Eksp. Teor. Fiz. **56**, 892 (1969)].
[21] F. Cano and B. Pire, Eur. Phys. J. A **19**, 423 (2004).
[22] S. Liuti and S. K. Taneja, Phys. Rev. C **72**, 034902 (2005).
[23] S. Liuti and S. K. Taneja, Phys. Rev. C **72**, 032201(R) (2005).
[24] V. Guzey and M. Strikman, Phys. Rev. C **68**, 015204 (2003).
[25] S. Scopetta, Phys. Rev. C **70**, 015205 (2004).
[26] S. Scopetta, Nucl. Phys. **A790**, 364 (2007).
[27] K. Goeke, V. Guzey, and M. Siddikov, Eur. Phys. J. A **36**, 49 (2008).
[28] J. R. Smith and G. A. Miller, Phys. Rev. C **65**, 055206 (2002).
[29] A. Kirchner and D. Mueller, Eur. Phys. J. C **32**, 347 (2003).
[30] M. V. Polyakov, Phys. Lett. **B555**, 57 (2003).
[31] J. Breitweg *et al.* (ZEUS Collaboration), Eur. Phys. J. C **6**, 43 (1999).
[32] C. Adloff *et al.* (H1 Collaboration), Z. Phys. C **76**, 613 (1997).
[33] A. Aktas *et al.* (H1 Collaboration), Eur. Phys. J. C **48**, 715 (2006).
[34] A. Aktas *et al.* (H1 Collaboration), Eur. Phys. J. C **48**, 749 (2006).
[35] J. C. Collins, Phys. Rev. D **57**, 3051 (1998); **61**, 019902(E) (2000).

[36] C. W. De Jager, H. De Vries, and C. De Vries, At. Data Nucl. Data Tables **36**, 495 (1987).
[37] T. H. Bauer, R. D. Spital, D. R. Yennie, and F. M. Pipkin, Rev. Mod. Phys. **50**, 261 (1978); **51**, 407(E) (1979).
[38] A. V. Radyushkin, Phys. Rev. D **56**, 5524 (1997).
[39] A. V. Belitsky, D. Mueller, and A. Kirchner, Nucl. Phys. **B629**, 323 (2002).
[40] L. Frankfurt, A. Freund, V. Guzey, and M. Strikman, Phys. Lett. **B418**, 345 (1998); **B429**, 414(E) (1998).
[41] K. Kumericki, D. Mueller, and K. Passek-Kumericki, arXiv:0807.0159 [hep-ph].
[42] V. Guzey and T. Teckentrup, Phys. Rev. D **79**, 017501 (2009).
[43] A. V. Belitsky, D. Müller, A. Kirchner, and A. Schafer, Phys. Rev. D **64**, 116002 (2001).
[44] V. Guzey, Phys. Rev. C **78**, 025211 (2008).
[45] K. Hencken *et al.*, Phys. Rep. **458**, 1 (2008).
[46] L. Frankfurt, V. Guzey, M. Strikman, and M. Zhalov, J. High Energy Phys. 08 (2003) 043.
[47] B. Pire, L. Szymanowski, and J. Wagner, Phys. Rev. D **79**, 014010 (2009); Nucl. Phys. B, Proc. Suppl. **179**, 232 (2008).